DANISH METEOROLOGICAL INSTITUTE

SCIENTIFIC REPORT

00-10

Evaluation of SSM/I Sea Ice Algorithms for use in the SAF on Ocean and Sea Ice

July 2000

Søren Andersen

Copenhagen 2000

ISSN 0905-3263 (printed version)
ISSN 1399-1949 (online version)
ISBN 87-7478-418-8

Summary

Within the frame of the EUMETSAT Satellite Application Facility (SAF) on ocean and sea ice a range of sea ice products are envisaged. The products encompass ice concentration mainly derived from Special Sensor Microwave/Imager (SSM/I) and possibly Advanced Very High Resolution radiometer (AVHRR) as well as ice edge and ice type based on multiple sensors combined in a Bayesian framework. The present report describes the study of passive microwave sea ice algorithms and parameters for use in the SAF project.

A set of 8 sea ice concentration algorithms are examined using a radiative transfer model and it is found that the NASA/TEAM algorithm displays the lowest sensitivities to geophysical noise over consolidated ice, whereas the Comiso Frequency mode algorithm is found to be most stable over open water. The findings are confirmed in a study of observed brightness temperatures and it is found that the stability of the concentration estimates is improved using the monthly tiepoints derived in the SAF project (Andersen, 1998). Consequently a weighting scheme to combine the two algorithms is devised. Different methods for removal of weather contamination are considered and a method which uses output from Numerical Weather Prediction (NWP) models to correct in brightness temperature space is described and assessed. When compared to traditional threshold based weather filters, it is found to provide more consistent concentration estimates at the ice edge, however it leaves more spurious ice. Thomas (1998) is proposing a conceptually similar procedure using retrievals over open water of the atmospheric parameters in stead of NWP model data. However, with his method it is necessary to extrapolate over the marginal ice, which may introduce artefacts. In light of this, it is concluded that the method should be evaluated along with the NWP based method using the validation data set based on navigational ice charts being built in connection with the SAF project. Finally, parameters for use in the SAF multisensor sea ice products are considered. As for ice type, it is concluded, based on the findings of Andersen (1998), that only the Gradient Ratio from 19 to 37 GHz is useful, given that it is corrected for the open water fraction. Regarding the ice edge, it is recommended to use the Comiso Frequency mode algorithm to provide a low noise estimate of the ice edge as well as the polarisation ratio at 85 GHz to benefit from the increased resolution at that frequency. The distribution of the 85 GHz polarisation ratio is close to gaussian, whereas the concentration estimate shows a large tail in the distribution. Following this, attempts are made to fit the generalised gamma distribution to histograms of Comiso Frequency mode concentration estimates, but the fitting procedure is found to be unstable. For operational applications the 2 parameter gamma distribution is found to provide good stability and reproduce the observed histograms well in most cases. Finally, monthly PDFs are found from original and atmospherically corrected brightness temperatures from 1999. It is found that for corrected brightness temperatures the fitting is less good during summer.

The present report can be seen as the conclusion of the algorithm development phase (Work Package 23110) as concerns the use of SSM/I. Work regarding the use of the Advanced Microwave Sounding Unit (AMSU) is currently in progress in connection with a visiting scientist exchange and will be described in a separate report. The outcome of this work will determine if AMSU data can contribute to any of the SAF sea ice products.

List of contents

1. Introduction

Within the frame of the EUMETSAT SAF on Ocean and Sea Ice, passive microwave radiometry is used for retrieval of the three sea ice parameters that are to be produced: ice edge, concentration and type. The ice edge product will be based on Special Sensor Microwave Imager (SSM/I), scatterometer and Advanced Very High Resolution Radiometer (AVHRR) data combined through a Bayesian technique described in Breivik et al. (1999). The concentration product will mainly be based on SSM/I with AVHRR contributing in cloudless, daylight conditions. The ice type product is to characterise the dominant ice type in terms of Multi Year (MY) and First Year (FY) ice, which is typically used as an indicator of ice thickness and will be based on combining SSM/I, scatterometer and AVHRR.

The SSM/I sensor on board the American Defence Meteorological Satellite Programme (DMSP) satellites, with its large coverage represents an essential source of data for all three products. This is particularly so for the concentration product, to which scatterometry is not able to contribute. Through the winter season, the SSM/I is typically able to deliver ice concentrations with less than 5 % error as demonstrated in this study. However, due to surface wetness during summer the performance is commonly experienced to deteriorate drastically. It is hoped that the ice analysis from AVHRR, that will probably function reliably in clear sky, daylight conditions may add information that can contribute to improve this shortcoming.

As for sea ice concentration, the approach taken is to optimise existing algorithms and select an algorithm or a combination of algorithms that deliver optimal results in terms of stability of the concentration estimate. A total of 8 algorithms have been selected for the comparative evaluation study. To that end use is made of Radiative Transfer Modelling (RTM) for sensitivity studies as well as evaluations of historical data over areas known a-priori to contain certain and stable surface types. The latter excludes the need for reference ice concentration data that will often have errors associated of at least the same magnitude as the SSM/I retrieval itself or introduce issues concerning the representativeness due to e.g. low spatial coverage.

To reduce the impact of residual sensitivity particularly to atmospheric water content and wind roughening of the sea surface, a simple radiative transfer model is employed using Numerical Weather Prediction (NWP) model fields as input to correct directly in brightness temperature space. This procedure is conceptually similar to the method proposed by Thomas (1998), where in stead of NWP data, the atmospheric information is retrieved from the SSM/I brightness temperatures over open water and extrapolated over the marginal ice. Using NWP data removes the need to extrapolate, but adds other error sources. Both methods have been developed in response to problems reported with the use of threshold based methods such as the NASA/TEAM and Bootstrap weather filters (e.g. Cavalieri, 1995; Comiso, 1997; Grumbine, 1996; Thomas, 1998)

A comparison of the two methods involves the inspection of often very slight differences and therefore requires comprehensive reference data, such as high resolution satellite imagery or navigational ice charts. Such a dataset is currently in the process of being collected within the

SAF project, consequently in this report it will only be possible to make preliminary considerations regarding the performance of the correction schemes.

Regarding the multisensor ice edge and type products, based on the findings from the sensitivity and evaluation study considerations are made as to which parameters can contribute with the most valuable information.

The report is laid out as follows: In section 2 the eight concentration algorithms considered are presented, in section 3 the correction scheme is introduced and initial studies of its usefulness and capabilities are reported in section 4. With this as a basis for assessing the significance of the findings, an RTM based sensitivity study is reported in section 5 and validated based on satellite measured brightness temperatures in section 6. Finally in section 7, based on the findings of the preceding chapters, considerations are made as to the use of SSM/I data in the multisensor ice edge and type products. Conclusions and recommendations are given in section 8.

2. Ice Concentration Algorithms

A total of 8 passive microwave ice concentration algorithms have been selected for analysis. These are:

1) NASA/Team (Cavalieri et al., 1984),
2) Bootstrap (Comiso, 1986) in polarisation mode,
3) Bootstrap (Comiso, 1986) in frequency mode,
4) Cal-val (Ramseier et al., 1991),
5) Norsex (Svendsen et al., 1983),
6) Bristol (Smith, 1996),
7) Near 90 GHz algorithm (Svendsen et al., 1987) and
8) TUD (Technical University of Denmark) improved resolution bootstrap algorithm (Toudal, 1998).

The first six of these algorithms use the low frequency channels of the SSM/I, while algorithms 7 and 8 make use of the higher resolution of the 85 GHz channels. The oldest algorithms (1, 2, 3 and 5) were originally developed for the channels featured by the SMMR and have been adjusted to work with the SSM/I channels. The most notable consequence is that moving the 18 GHz SMMR channel to 19.3 GHz on the SSM/I has brought a somewhat higher sensitivity to atmospheric water vapour as the SSM/I channel is closer to the 22.2 GHz water vapour absorption line.

Due to the commonly experienced problem of atmospheric contamination of the concentration retrievals, many of the algorithms are equipped with so called weather filters, all of which are based on thresholds on various SSM/I observed parameters. Some drawbacks are related to such procedures: The filters typically limit the ability of the algorithms to measure ice concentrations below 15% and they are known to saturate in cases of very heavy cloud and precipitation as well as to sporadically trigger within the ice pack (Grumbine, 1996). For obvious reasons the mixture of sea ice and weather related contamination found in the marginal ice zone can not be handled adequately with such threshold based filters.

Consequently, as documented in chapter 3, we explore the use of auxiliary information to enable more accurate corrections. In addition to this, weather filters are omitted in the study to evaluate the performance of the algorithms on equal terms.

A short summary of each algorithm is given below:

2.1 NASA/TEAM algorithm

The NASA/TEAM algorithm uses the fact that the polarisation difference is much smaller for ice than for water and that the spectral gradient is numerically small for first year ice, negative for multi year ice and positive for open water. Furthermore the influence of the physical temperature is reduced by the definition of normalised polarisation and gradient ratios (PR and GR, respectively):

$$PR(f) = \frac{T_B(f,v) - T_B(f,h)}{T_B(f,v) + T_B(f,h)}$$
$$GR(f_1, f_2, p) = \frac{T_B(f_2,p) - T_B(f_1,p)}{T_B(f_2,p) + T_B(f_1,p)} \quad (1.)$$

with brightness temperatures symbolised by $T_B(f,p)$, where f is frequency and p is polarisation. Assuming a mixture of open water, first year ice and multi year ice within the footprint of the satellite ($C_{FY}+C_{MY}=C_T$=total concentration) the partial concentrations may be inferred from:

$$C_{FY} = \frac{F_0 + F_1 PR + F_2 GR + F_3 PRGR}{D}$$
$$C_{MY} = \frac{M_0 + M_1 PR + M_2 GR + M_3 PRGR}{D} \quad (2.)$$
$$D = D_0 + D_1 PR + D_2 GR + D_3 PRGR$$

where PR=PR(19) and GR=GR(19,37,V). The coefficients F, M and D are based on observed brightness temperatures and therefore depend on the microwave sensor used. This algorithm, as opposed to the other algorithms, is mildly non-linear in terms of brightness temperature. It has been extensively tested within the scientific community, thus its performance is well documented. For use in areas that do not contain MY ice, a variation of the NASA/TEAM algorithm has been developed, essentially replacing the MY tiepoint with a tiepoint corresponding to new ice (Cavalieri, 1994). This algorithm is essentially the only one existing which explicitly takes into account the presence of new ice types and it may be used in such areas as the Baffin Bay and the Baltic Sea, as well as in the Northern Pacific. It is not specifically treated in the following, this is left to a coming validation study including navigational ice chart information.

2.2 Comiso Bootstrap algorithms

The bootstrap algorithm is based on the observation of linear clustering of consolidated ice in scatter plots of $T_B(37,v)$ against $T_B(37,h)$ and $T_B(37,v)$ against $T_B(19,v)$, whereas points of open water tend to cluster about a single point. For the determination of total ice concentration this algorithm has several advantages. It assumes that atmospheric effects are part of the data set, while minimising the effects of surface temperature. It assumes only two types of surfaces (sea ice and open water) taking into account the variability of both to optimise the detection of small ice concentrations. Furthermore it allows higher resolution to be obtained through the use of 37 GHz data at the expense of increased vulnerability to snow cover and atmospheric interference. The linear relationship, yields the following simple formalism:

$$C_T = \frac{T_B - T_B^W}{T_B^I + T_B^W} \quad (3.)$$

where superscript W signifies a water tie point and superscript I signifies the calculated brightness temperature of ice. This equation is solved by using either 37 GHz measurements

in two polarisations or 37 and 19 GHz in vertical polarisation mode. Comiso et al. (1986) proposes that the polarisation method be used in the perennial ice zone (concentrations larger than 90 %), while in the rest of the domain the frequency scheme is used to decrease atmospheric distortion and increase the discrimination between ice and open water. This switching may, however, introduce discontinuities (Smith et al., 1995) and in the frame of the present project the two modes will be studied separately.

2.3 Cal-val algorithm

The Cal-Val algorithm was developed for the calibration-validation study in connection with the first DMSP mission carrying the SSM/I sensor. It is a simplified version of the AES-York algorithm and both of these algorithms are described in Ramseier et al. (1991), who quotes the errors in the concentration retrieval of the two algorithms to be similar. Essentially, the algorithms express the ice concentration as a linear combination of the V-polarised SSM/I channels at 19 and 37 GHz, where the coefficients are chosen from two sets depending on the season:

$$C_T = C_1 \cdot T_B(37,v) + C_2 \cdot T_B(19,v) + C_3 \qquad (4.)$$

i.e. there exists two sets of $\{C_i \mid i=[1,3]\}$.

This simple linear relation is exposed to a considerable source of error from surface temperature fluctuations if these are not corrected for otherwise.

2.4 Norsex algorithm

The NORSEX algorithm (Svendsen et al., 1983) attempts to remove the atmospheric contributions to the brightness temperature measured at the space craft to facilitate the use of tie point emissivities obtained from the surface during the NORSEX experiment. Using a simplified radiative transfer equation, the effective net brightness temperature at the surface T_B^E is given by:

$$T_B^E = \frac{T_B^A - 2\delta T_{atm}\tau + \delta T_{atm}\tau^2 - T_B^{sp}}{1 - \tau - \beta\delta(\tau - \tau^2) - \beta(T_B^{sp} / T_B^A)} \qquad (5.)$$

where T_B^A is the brightness temperature sensed at satellite height, δT_{atm} is the weighted average atmospheric temperature, T_B^{sp} is the brightness temperature from deep space, τ is the atmospheric opacity (see equation 4) and β and δ are constants close to unity. The atmospheric opacity is assumed to depend linearly on atmospheric temperature between 250 and 270 K, although, as the authors admit, the opacity varies considerably with other conditions. Assuming a mixture of 3 principal surfaces, the emitted brightness temperature may be written

$$T_B^E = (e_{MY} C_{MY} + e_{FY} C_{FY}) T_I + e_W C_W T_W \qquad (6.)$$

where T_I and T_W is the physical surface temperatures of the ice and water, respectively. Provided the surface air temperature is known, the ice temperature is computed by

$$T_I = aT_A + (1-a)T_W \qquad (7.)$$

where T_A is the surface air temperature and a (=0.4) has been determined from analysis of buoy temperatures and the water temperature is assumed to be 272 K. With 19 and 37 GHz vertical polarisation data C_{MY} and C_{FY} can be estimated. This total concentration is then used to interpolate between surface temperature over water and ice to reach a new and improved ice concentration estimate.

2.5 Bristol algorithm

The Bristol algorithm (Smith, 1996) is conceptually similar to the Bootstrap algorithm in that it uses the fact that data plotted in a three-dimensional scatter plot tend to lie in a plane. The only difference is that instead of viewing the data in e.g. a $T_B(37,v),T_B(37,h)$ plane, the Bristol algorithm views the data perpendicular to the plane in which it lies, i.e. in a co-ordinate system where the axes are:

$$\begin{aligned} &1\text{: } T_B(37,v) + 1.045T_B(37,h) + 0.525T_B(19,v) \\ &2\text{: } 0.9164T_B(19,v) - T_B(37,v) + 0.4965T_B(37,h) \end{aligned} \qquad (8.)$$

With this observation, the remaining analysis is identical and the advantage of the Bristol algorithm as compared to the Bootstrap algorithm, is a larger retrieval triangle and therefore in theory less noisy, more stable retrievals.

2.6 Near 90 GHz algorithm

The 90 GHz ice concentration algorithm by Svendsen et al. (1987) uses the observation that the difference in emissivity between horizontal and vertical polarisation is small for first year and multi year ice types, but large for open water. It incorporates a correction for atmospheric effects by the use of a smooth function of the ice concentration with tie points over open ocean and 100 % ice for each orbit. This method rests on the assumption that the atmospheric opacity is a function of atmospheric temperature, which clearly depends on ice concentration. Of course the assumption is violated in many cases, as in the presence of weather fronts. Also the selection of tiepoints for each orbit for the weather correction scheme is not trivial as the highest or lowest polarisation may not necessarily be representative of water or ice, respectively. In many cases this selection is probably best done interactively.

2.7 TUD improved resolution bootstrap algorithm

The TUD (Technical University of Denmark) improved resolution algorithm is described by Toudal (1998). The ice concentration is simply expressed as the product of the Comiso bootstrap frequency mode algorithm and a linear expression involving the polarisation difference, $P=T_B(85,v)-T_B(85,h)$:

$$C_T = \sqrt{C_{low} \cdot (A \cdot P + B)} \qquad (9.)$$

where C_{low} is the estimate from the Comiso bootstrap frequency mode algorithm, while A and B are constants that may readily be determined from tiepoint emissivities. The resulting resolution, although poorer than the 85 GHz, is better than that of the generic bootstrap algorithm, while the noise inherent in the 85 GHz channels is suppressed quite efficiently. One reason for choosing the Comiso frequency mode algorithm as a background is its low sensitivity to atmospheric noise, as will be demonstrated in chapter 4. In the actual implementation, a concentration threshold can be chosen, below which the algorithm relies solely on the low resolution concentration retrieval. This will often make sense, as over open water, atmospheric disturbances are generally much larger than over consolidated ice. In this study the threshold is set to C_T=10 %.

3. Correction of atmospheric contamination

As mentioned earlier there are drawbacks connected with the use of the well known threshold based weather filters such as those proposed by Cavalieri et al (1995) and Comiso et al. (1997). Furthermore, these filters are not particularly useful in the multisensor scheme to be used for ice edge and type analyses and for these two main reasons alternative methods are investigated. It is evident that auxiliary information concerning the atmospheric state is needed. Thomas (1998) suggested using retrievals of water vapour (v), cloud liquid water (clw) and wind speed at 10 m (w) from SSM/I brightness temperatures over open water, extrapolating across the marginal ice zone. He demonstrated a significant improvement and very efficient elimination of atmospheric contamination. However, the extrapolation over the marginal ice may introduce artefacts. Therefore in the frame of the present project, to avoid the extrapolation and enable a correction over consolidated ice as well, we will attempt to take the atmospheric information from Numerical Weather Prediction (NWP) models. As a first step we compare NWP parameters and SSM/I retrievals to determine whether the current NWP parameters are sufficiently accurate for the intended use. Subsequently we describe the correction scheme to finally make comparisons to the NASA/TEAM weather filter.

3.1 Comparison of NWP and retrieved parameters

To investigate how well the NWP model representation of the atmospheric water content and surface wind corresponds with observed SSM/I brightnesses an entire month of SSM/I data covering the North Atlantic were evaluated against NWP fields. The SSM/I brightness temperatures were converted to clw, v and w using algorithms by Karstens et al. (1994), Simmer (1994) and Lo (1983), respectively. Following the elimination of land and coastal pixels, these same quantities were extracted for each SSM/I pixel from the closest analysis or short forecast of the HIRLAM NWP model running at DMI (Sass et al., 1999). The resulting statistics are shown in table 1 below.

	Wind (w)		**Water vap. (v)**		**Cloud liq. wat. (clw)**	
	Corr.	Std. dev.	Corr.	Std. dev.	Corr.	Std. dev.
Mean	0.71	2.91	0.85	0.72	0.38	0.15
Min	0.52	0.90	0.54	0.52	-0.03	0.04
Max	0.85	6.01	0.95	4.03	0.72	0.29

Table 1 *Correlation between NWP model parameters and corresponding SSM/I based retrievals as well as standard deviations of the differences during April 1999. First row gives the statistics of all pixels in this period, whereas the next two rows are the extreme correlations of individual SSM/I passes. Units of the standard deviations are m/s for wind and* kg/m^2 *for the water vapour content and cloud liquid water.*

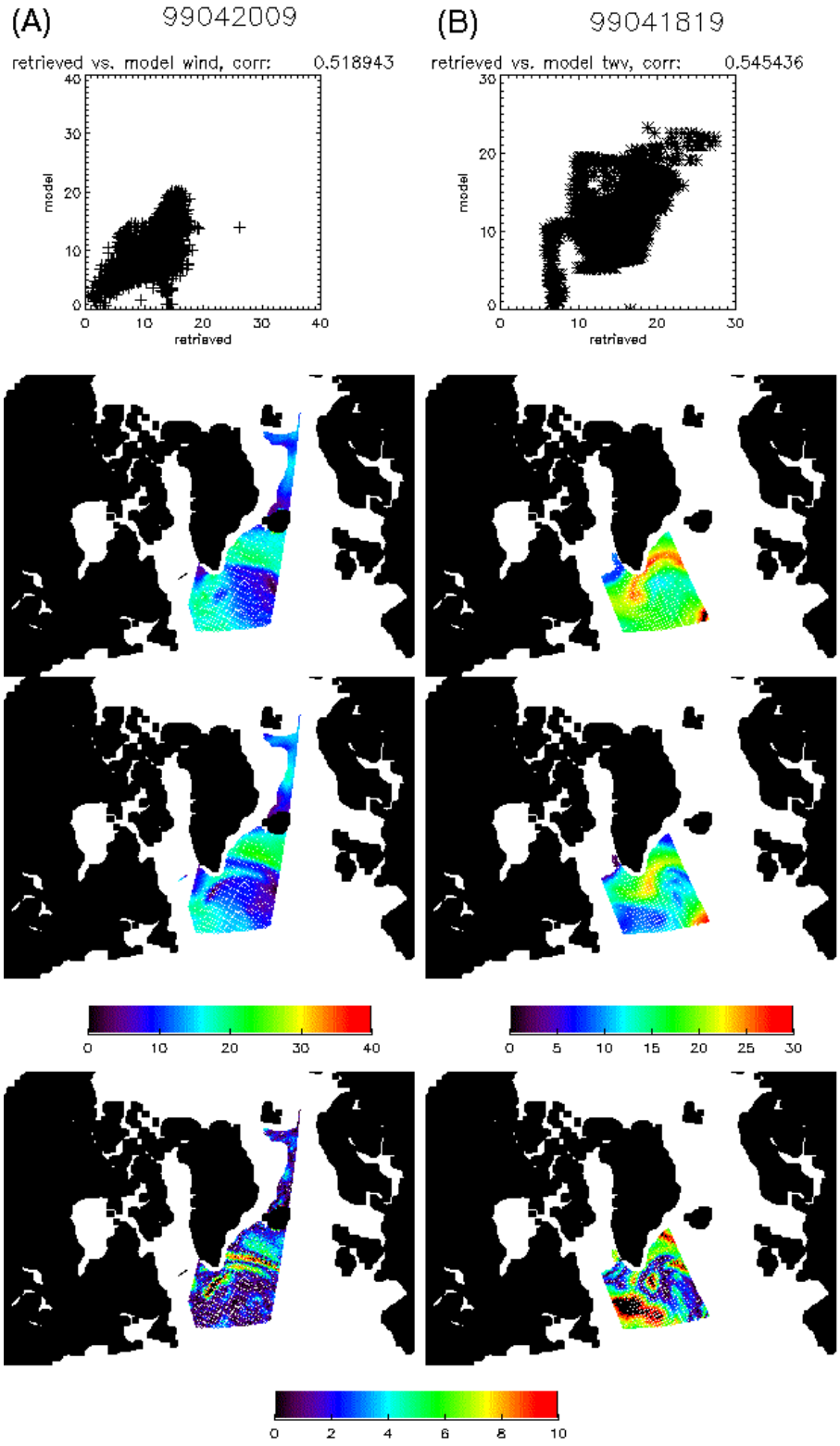

Figure 1 Comparisons of retrieved vs. model atmospheric parameters. Column A) displays wind and column B) displays water vapour fields for the swath displaying the minimum correlation between model and retrieved parameters. The maps display from the top down the retrieved parameter, the model parameter and difference between retrival and NWP model.

It is seen that, on average, acceptable statistics are obtained for w and v, whereas the cloud liquid water information in the NWP model compares very poorly with the SSM/I retrievals. Using this parameter in a correction scheme is risky and therefore we do not take it into account in the following. However to explore how the uncertainty of the remaining parameters is distributed and how it translates into errors in the ice concentration analysis, further examination is required. Plots comparing the distributions of total water vapour and wind speed at the minimum correlation is shown in Figure 1 (next page). It is seen that the general features are present in the NWP fields but are different in shape. The maximum difference can be more than 10 m/s for wind and more than 10 kg/m^2 for water vapour, which will clearly result in considerable residual error on the concentration map. In the two following sections the NWP model data will be applied in a correction procedure and the two passes in Figure 1 will be taken as the worst case situation to give an indication of the performance that can be expected from a correction procedure using NWP data.

3.2 Correction scheme

At the frequencies of the SSM/I, the radiative transfer of microwave radiation can be written as the sum of contributions from surface emission, reflection of atmospheric emission and radiation from deep space as well as direct atmospheric emission. All of these terms are subject to atmospheric extinction and scattering. At frequencies below 50 GHz (Ulaby et al., 1981) scattering effects are negligible and the radiative transfer problem is relatively easy to solve. However, at frequencies above 50 GHz or in case of rain, scattering effects become important and requires greater resources for the solution of the radiative transfer problem with sufficient accuracy.

The scheme to be used for correcting the SSM/I brightness temperatures is depicted in Figure 2. Given the NWP model estimate of surface temperature, v and w a correction can be calculated using a radiative transfer model (RTM) and applied to the measured SSM/I brightness temperatures in each pixel. At each SSM/I pixel location NWP model data are interpolated and extracted from the closest analysis or short forecast. Based on this a predicted brightness temperature representative of the NWP model representation of the atmospheric state is computed (blue path in Figure 2). To avoid problems pertaining to lack of absolute calibration of the RTM, another RTM calculation is performed to estimate the predicted brightness temperature of a reference atmospheric state (green path in Figure 2). For concentration retrieval, using tiepoints developed within the SAF project (Andersen, 1998), this state is known and equivalent to climatology. The advantage of this method is that no constraints are imposed on the choice of parameters to enter into the multisensor products based on the Bayesian approach, while the concentration retrieval is kept consistent with the tiepoints.

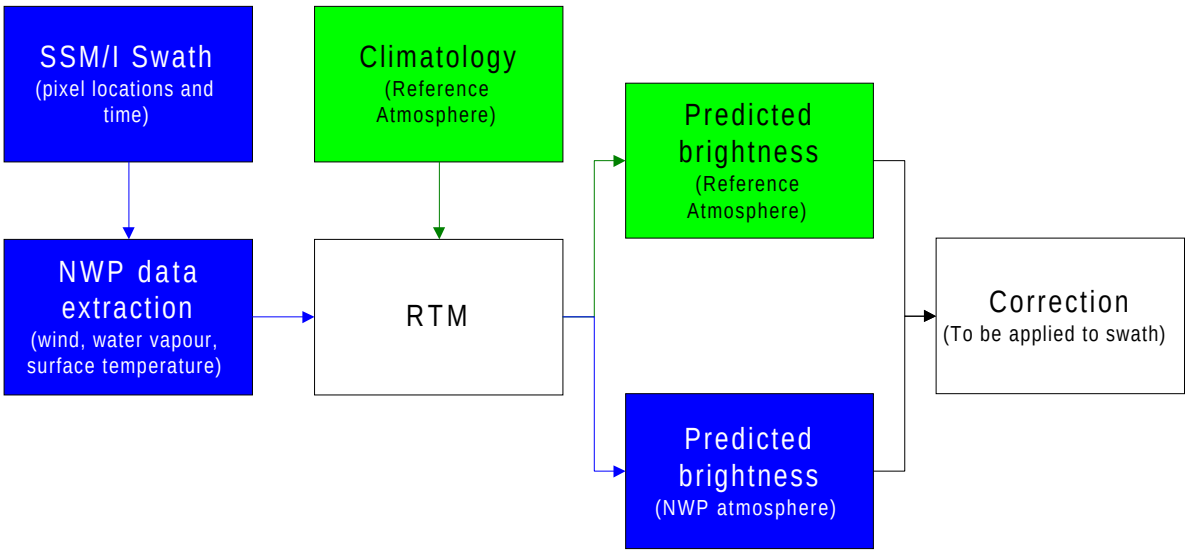

Figure 2 Block diagram of a correction scheme using NWP model parameters. The colors green and blue indicate the paths of climatological and NWP model data.

To handle the radiative transfer calculations at the lower SSM/I frequencies the fast radiative transfer model described in Wentz (1997) has been selected and is feasible to run for every pixel of a swath, whereas for the 85 GHz channels lookup tables have been prepared by Kern (1999) using the accurate RTM, MWMOD (Fuhrhop, 1997).

Evidently, the surface emissivity and thereby the radiative transfer budget is affected by the ice concentration. A special handling of the ice concentration estimate in the radiative transfer calculations therefore has to be performed. The strategy chosen is illustrated in Figure 3, where the concentration equivalent correction for different values of w and v is depicted against the ice concentration with which the radiative transfer calculations are performed. The concentration equivalent correction is defined as the ice concentration computed from the predicted brightness temperature for an atmosphere with certain levels of total water vapour content (v) and wind (w) minus the ice concentration computed from the predicted brightness temperature of a clear atmosphere: $\Delta C = C(T_B(w,v)) - C(T_B(0,0))$. Initially, the observed brightness temperatures are used in conjunction with an ice concentration algorithm, in the present case NASA/TEAM, to estimate the ice concentration, C_0, that goes into an initial correction calculation. It is clear that this concentration estimate will be affected by atmospheric contamination and the result is therefore unrealistic. However, using the obvious near linear behaviour of the correction as function of ice concentration, it is possible to arrive at an ice concentration value that is consistent with the atmospheric state. To characterise the slope of the correction curve in Figure 3, the initial correction is applied to arrive at a first shot corrected ice concentration, C_1. This value will generally be too high and based on C_1 a second correction is calculated and applied giving the second corrected concentration estimate C_2. Defining the two corrections:

$$\Delta C(C_n) = C_n - C_{n+1} \mid n \in \{0,1\} \qquad (10.)$$

The correction curve in Figure 3 is a straight line and can be written as:

$$\begin{aligned} \Delta C(C) &= \alpha \cdot C + \beta \\ \alpha &= \frac{\Delta C(C_1) - \Delta C(C_0)}{C_1 - C_0} \\ \beta &= \Delta C(C_1) - \alpha \cdot C_1 \end{aligned} \qquad (11.)$$

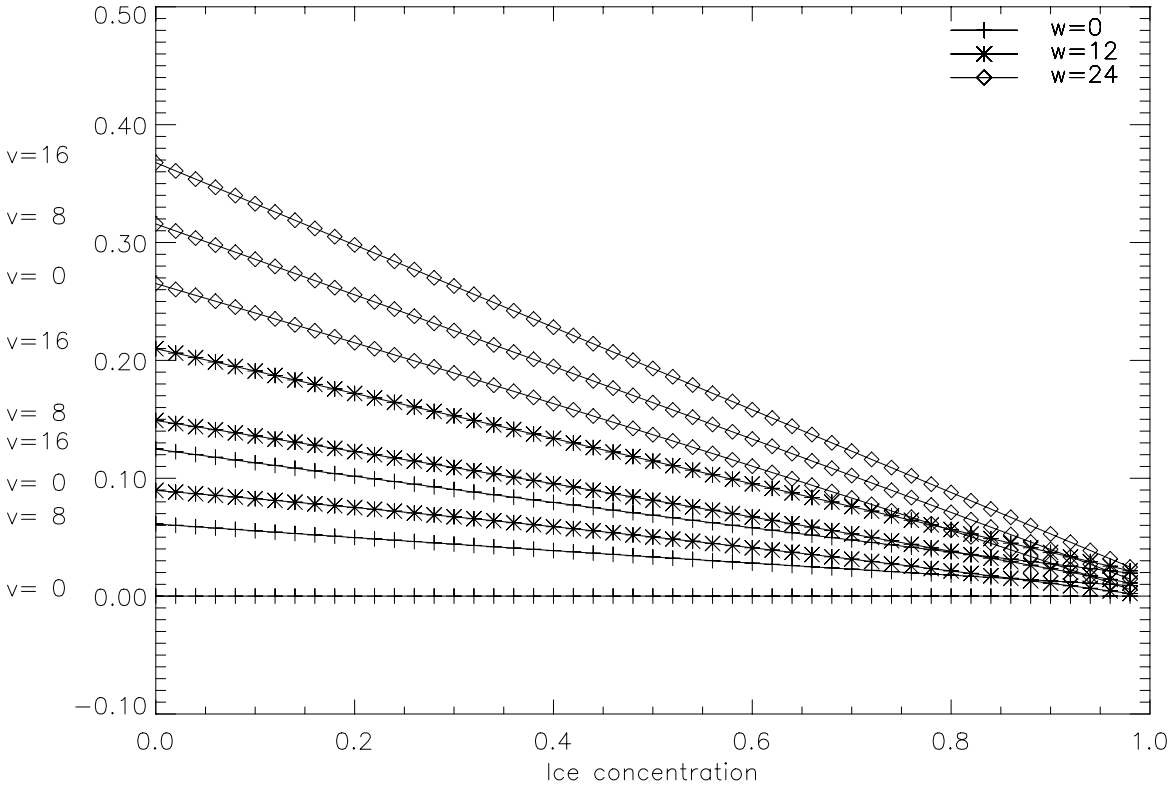

Figure 3 Plot of concentration equivalent corrections using NASA/TEAM (see text for definition) as function of the ice concentration assumed in the radiative transfer calculations for varying values of wind (w) and total water vapour (v).

For the concentration consistent with the atmospheric state, $C=C_{true}$, the calculated correction, C_0-C_{true} must be equal to the value of $\Delta C(C_{true})$. Together with equation 10 and 11, this requirement yields:

$$C_{true} = \frac{C_0 - \beta}{1 + \alpha} \qquad (12.)$$

The choice of ice concentration algorithm is not critical to the success of this method as trials show they all display the near linear behaviour shown in Figure 3.

4. Performance of the NWP model based correction

To give a preliminary estimate of the performance of the NWP model based correction, its impact on ice concentration retrievals are considered in this chapter relative to the NASA weather filter. Clearly, the performance of the NWP model based correction scheme is dependent on the quality of the meteorological data. As a minimum, the correction scheme must be able to reduce the variance of ice concentration retrievals over open water. To demonstrate this, the correction was applied to all swaths available during the month of April 1999 and statistics of ice concentration retrievals were calculated over a 5x5° open water area.

	Without correction				**With correction**			
	Mean (%)		**Std. dev. (%)**		**Mean (%)**		**Std. dev. (%)**	
NASA TEAM	(6.4)	1.1	(5.52)	5.52	(2.4)	-2.7	(3.10)	3.24
Bootstrap Polarisation Mode	(22.7)	3.3	(12.91)	13.90	(16.0)	-3.9	(10.10)	10.83
Bootstrap Frequency Mode	(-2.0)	2.5	(3.32)	3.39	(-5.7)	-0.6	(2.38)	2.04

Table 2 *Statistics for a timeseries spanning the month of April 1999 of ice concentration retrievals with 3 different algorithms using corrected or uncorrected SSM/I brightness temperatures. Statistics for concentrations calculated using tiepoints supplied by the original authors are given in parantheses, all other values are based on the tiepoint set described in the present report.*

For the purpose of demonstration, only the two Bootstrap algorithms and the NASA/TEAM algorithms results are shown in table 2 and show a significant improvements in the variance of the retrievals. However, the dependence on the algorithm sensitivity to atmospheric influences is evident in the bootstrap polarisation mode results and underlines the importance of selecting the concentration algorithm such that the sensitivity is minimised.

To demonstrate the worst case performance of the correction technique as compared to conventional weather filtering, the two low correlation swaths shown in section 3.1 are converted to ice concentration and compared to ice concentrations with either no corrections and ice concentrations filtered using the NASA weatherfilter. The result is shown in the two leftmost columns of Figure 4, note that the Bering Sea and the Sea of Okhotsk are outside the domain of the NWP model used and therefore the NWP corrected concentration estimates there are not correct. As expected the correction scheme is not able to remove all contamination, although a significant improvement is evident. In this case the conventional weather filtering technique seems to outperform the NWP correction scheme, however a close inspection of the ice edges of e.g. the Baffin Bay and the East Greenland Coast shows that the lowest ice concentrations are removed by the conventional filtering scheme as it is also reported by e.g. Cavalieri et al. (1995). Occasionally, the conventional weather filtering approach may be presented with severe weather effects that cause it to saturate. One example is given in the rightmost column of Figure 4, where a tongue of severe weather contamination is protruding in the Southern part of Greenland. Here the NWP approach suppresses the weather contamination and performs as well as the conventional filtering. Although this sort of situation is relatively rare it shows that even the use of standard threshold based

weather filtering may allow large weather related disturbances to propagate into the concentration maps.

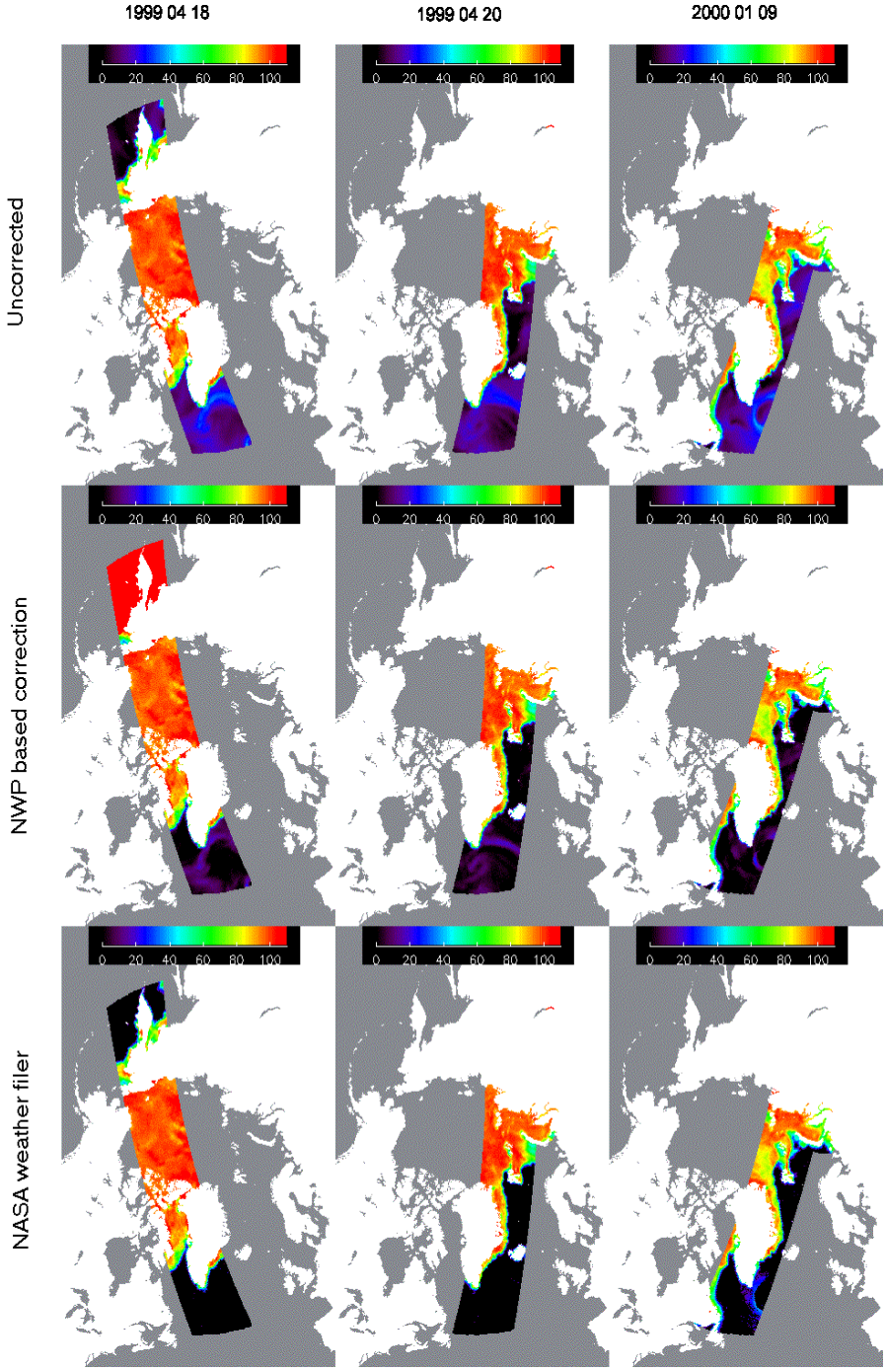

Figure 4 Maps of ice concentrations from top to bottom: uncorrected, corrected using the NWP correction scheme and corrected using the NASA weather filter. The two leftmost columns represent the worst case identified in section 3.1, while the rightmost column is a recent example of the NWP correction method performing at least as well as conventional weather filtering.

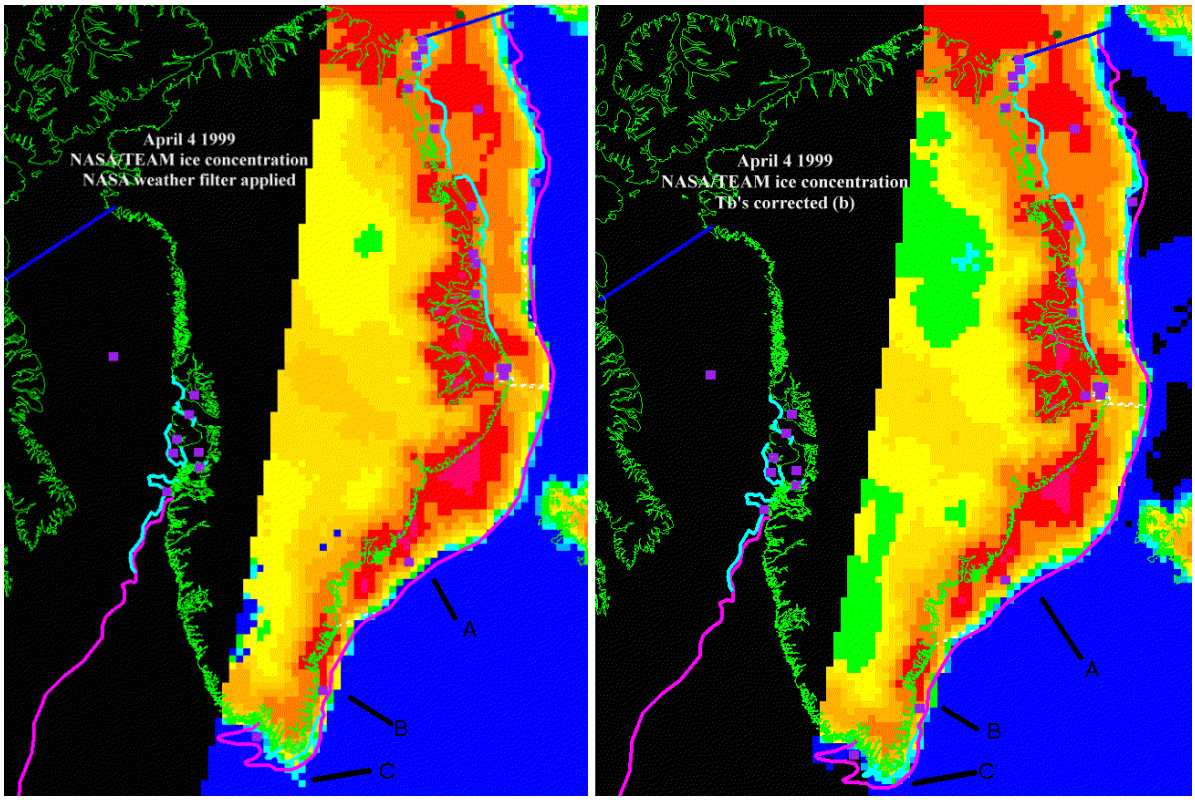

Figure 5 Maps of ice concentrations corrected using the NASA weather filter (left) and using the NWP based correction scheme (right). Overlaid in cyan is the DMI navigational ice analysis based on SSM/I, AVHRR and Radarsat. It is obvious that ice is falsely discarded by the NASA weather filter southwest of Iceland. Areas discussed in the text are marked A, B and C.

In practice, the possibility of loss of information is of great concern. By close inspection of the Davis Strait area in Figure 4 it is clear that low concentration pixels are preserved using the NWP based correction, while they are generally completely removed by the NASA weather filter. Similar, although milder, problems are illustrated in detail in Figure 5 where ice concentration maps corrected using the NASA weather filter and the NWP correction method are compared to the ice edge drawn by analysts at DMI based on SSM/I, AVHRR and Radarsat. It should be noted that as the pixels are 25x25 km, differences involving a single pixel translate into a considerable area and are therefore significant. The differences are especially obvious southwest of Iceland, where three features are marked by black line symbols. The concern that information may be lost using the NASA weatherfilter is confirmed at the most northerly marking (A) where the NWP corrected field follows the ice edge more closely. Also it is obvious how using thresholdbased methods precludes corrections in the marginal ice zone, thus at the second marking (B) the concentrations in NWP corrected map are lower and more realistic. At the third marking (C), around Cape Farewell the NASA weatherfilter is clearly saturated and a contamination feature extends around 50 km into the open ocean. In the Northerly part of the image, the differences between NASA filtered and NWP corrected concentration estimates are negligible.

In conclusion, the assets of threshold based methods versus the correction methods outlined in this report must be weighted against the drawbacks attached to them. It is clear that the NASA weatherfilter over open water is more likely to filter out atmospheric contamination completely. However, with the very complicated radiative conditions at the marginal ice zone, thresholding is clearly not adequate and errors are easily introduced, occasionally resulting in loss of information and at any rate resulting in non-optimal concentration estimates at low and intermediate concentrations. The NWP based correction scheme suffers from occasional poor quality of the atmospheric fields and is more often unable to screen out all atmospheric contamination. The method of Thomas (1998) does not suffer from this shortcoming but the extrapolation step may have unfortunate effects. In light of these findings a feasible way to proceed for the SAF project is to investigate the reliability of the method of Thomas (1998) as compared to the NWP based method and threshold based weather filters using the comprehensive validation data set presently being built at DMI and DNMI. The outcome of this study will be included in a coming report on the validation of the SAF sea ice product. At any rate, it is unproblematic to incorporate the method of Thomas (1998) in the present scheme as it only involves a change of the source of atmospheric information from NWP based to retrieval based. The first priority, however, should be to minimise the sensitivity of the concentration retrieval algorithm to the atmospheric influences. This will be considered in the next chapters.

5. Sensitivity of concentration algorithms

The preceding section has shown that residual geophysical noise (atmospheric contamination) can contribute large errors to the retrieved sea ice parameters. Therefore it is very important that the selected concentration algorithm has low sensitivity to the sources of geophysical noise. To ensure this, and to obtain a good basis for the choice of algorithms and parameters for use in the SAF project, an analysis consisting of an RTM based sensitivity study has been undertaken, followed by an evaluation study on real observations to confirm or reject the findings. In this section, the method and findings of the theoretical sensitivity study are given, while the evaluation study is reported in section 5.

5.1 Method

Using the RTM MWMOD (Fuhrhop, 1997), simulated brightness temperatures were calculated for varying wind (only at 0% ice concentration), total water vapour, cloud liquid water, surface temperature and ice concentration (surface emissivity). MWMOD is a general RTM and solves the complete radiative transfer problem using the successive order of scattering method with polarisation dependent Mie-scattering and cloud parameterisation. For establishing the sensitivity to wind over open water, the emissivity of the wind roughened surface, was parameterized using a 3-scale model (Schrader, 1995) and the atmosphere was kept clear. The sensitivities to cloud liquid water and total water vapour content were examined with varying ice concentration. This was done by setting the surface emissivities according to the ice water mixture using the SAF tiepoints for January, corrected to calm clear atmospheric conditions using climatological mean wind and water vapour content. Both MY and FY ice surfaces were taken into account. Finally, cloud liquid water was varied by changing the hydrometeor density of a fixed cloud layer of 1 km thickness.

5.2 Results

Plots of the sensitivities resulting from the analysis described above are given in Appendix A. For ice covered surfaces, three experiments are made with different ice surface emissivity and ice temperature. Additionally an experiment is conducted assuming an open water surface while varying the wind conditions. In the following, algorithms are referred to by their respective numbers as defined in section 2, when most convenient.

5.2.1 Total water vapour

As for the sensitivities to total water vapour, the results are relatively similar for all of the algorithms that do not use the 85 GHz SSM/I channels. As a rule of thumb the sensitivity to water vapour grows proportional to frequency squared and this is clearly reflected in the results for the Near 90 GHz algorithm, whereas the TUD hybrid algorithm succesfully reduces the high noiselevel of the 85 GHz channels. The obvious discontinuity of the 0% line is due to the selection of the 10% threshold, mentioned in section 2.7. The temperature dependence of the algorithms is revealed in the Case 3 plots, where the temperature of the emitting ice layer has been reduced by 4 K. Following Svendsen et al., 1983, this is equivalent to a 10 K reduction in air temperature. As expected the NASA/TEAM, Comiso polarisation mode and the Near 90 GHz algorithms are largely insensitive, displaying a decrease in concentration estimates of max. 1%. The rest of the algorithms display concentration changes between 2 and 4 %.

5.2.2 Cloud liquid water

When it comes to the sensitivities to cloud liquid water, the differences between the algorithms are much larger. As the correction scheme described earlier does not take that quantity into account, this is a very important finding. The results can be separated in the part over open water and the part over consolidated ice. Over open water, the algorithms that use horisontally polarised channels (1,2,6,7,8) are found to be very sensitive to cloud liquid water. Especially algorithms 2 and 7 display the largest errors due to the use of higher frequency information. Over FY ice differences are slight, however over a low emissivity MY ice surface large sensitivities are found for algorithms 2 through 7, which is clearly limiting their usefulness. At last, the sensitivities to wind roughening again, as expected, reveal large errors for the algorithms using h-polarised channels.

5.2.3 Wind

The last plot in Appendix A shows the sensitivities of the concentration algorithms to wind roughening of the sea surface. Most significantly, the sensitivities depends on whether a horisontally polarised channel is used. Thus algorithms 1, 2, 6, 7 and 8 with their use of horisontally polarised channels are exposed to large sensitivities, while the remaining algorithms are virtually unaffected. In particular this is unfortunate for the Bristol algorithm, where the change of retrieval geometry introduces a larger sensitivity to wind.

5.2.4 Overall performances

To obtain a quantitative measure for the overall sensitivities of the algorithms, in analogy with the analysis presented by Pedersen (1991), total sensitivities are calculated based on climatological standard deviations in the physical parameters influencing the radiative transfer. To facilitate comparisons, the values used by Pedersen (1991) are adopted with minor modifications as shown in table 3 even though, as pointed out by Oelke (1997), the maximum cloud liquid water (clw) value of 0.1 kg/m^2 is on the low side. Oelke (1997), from radiosounding ascents in the Southern Ocean finds mean values of clw between 0.17 and 0.29 kg/m^2 depending on latitude. From NWP model data and retrievals close to the ice edge, similar values are found in this study, see section 3.1.

	Mean	**Standard deviation**
clw (kg/m^2)	0.0	0.07
wind (m/s)	8.0	5.0
water vapour (kg/m^2)	4.0	5.5
Air temperature (°C)	-5.0	8.0
SST (°C)	-1.0 (-1.75)	2.6

Table 3 *Mean values and variability of parameters used to calculate total sensitivities taken from Pedersen (1991). For SST a slightly different mean SST is used, the original value is given in parantheses.*

Evidently values obtained based on the quantities given in table 3 are not useful for estimating the performance of the algorithms based on atmospherically corrected brightness temperatures. Therefore additional sensitivities are calculated based on the values given in table 1. In line with Pedersen (1991), the sensitivity is computed as the change in ice concentration resulting from a positive change in a given parameter of one standard deviation from the

mean value. Assuming the variations are independent, total sensitivities are subsequently calculated as the square root of the sum of squares of the individual sensitivities. For the computation of the total sensitivity, in lack of better knowledge it is conservatively assumed that the use of SST and air temperature from NWP models can halve the error in ice concentration associated with variations in that parameter. Similarly, as cloud liquid water information is not used in the NWP correction, the sensitivities corresponding to uncorrected data is used. The results are shown in tables 4-6 for open water, FY and MY surfaces, respectively. The tables are meant as a support for assessing the significance of the plots shown in appendix A and the results are reasonably well in accord with the measured sensitivities given in table 2. It should be kept in mind, however, that particularly the non-gaussian distribution of the wind combined with the non-linear behaviour of the sensitivities to wind for many algorithms will result in higher typical sensitivities than those shown in tables 4-6. Similarly the somewhat low variation in cloud liquid water used here will lead to underestimation of the actual significance of that parameter as well as of the total sensitivities.

The almost identical performance of algorithms 3, 4 and 5 could be expected as they all use the same channel combinations and only differ in different approaches to compensation for atmospheric influences. In that respect, the Comiso approach represents a good compromise between simplicity and efficiency compared to the more complicated NORSEX and the simplistic cal-val algorithms. The performance of the Bristol algorithm is disappointing as it seems to inherit the large sensitivity over open water from the use of horisontally polarised information while keeping the sensitivity to cloud liquid water over low emissivity ice surfaces that characterises the Comiso frequency mode algorithm. The improved resolution of the algorithms using the 85 GHz channels is largely countered by very large sensitivities to both wind, water vapour and cloud liquid water although the TUD algorithm manages to produce results at least on the level of the Comiso Polarisation mode algorithm. However, when the objective is accurate ice concentration estimates, especially in the marginal ice zone, the errors that are likely to be introduced are unacceptable. Consequently, the most promising algorithms from this study would be the NASA/TEAM algorithm that shows an unequalled stability over high ice concentrations as well as the Comiso frequency mode algorithm that shows the lowest sensitivities to virtually all atmospheric contamination sources over open water. In the following section, to validate the results obtained here, the study will therefore be narrowed to take into account only these two conventional algorithms.

Alg. No.	clw		wind		water vap.		SST		Total	
	Orig	Corr	Orig	Corr	Orig	Corr	Orig	Corr	Orig	Corr
1	1.05	2.25	1.50	0.87	4.47	0.59	0.0	-	4.83	1.49
2	7.88	16.9	12.5	7.28	4.81	0.63	-1.1	-	15.6	10.8
3	-0.18	-0.38	-1.50	-0.87	4.47	0.59	1.4	-	4.92	1.28
4	-0.18	-0.38	-2.00	-1.16	4.13	0.54	1.4	-	4.80	1.47
5	-0.35	-0.75	-2.00	-1.16	4.13	0.54	1.4	-	4.81	1.50
6	2.45	5.25	3.00	1.75	4.47	0.59	1.3	-	6.05	3.14
7	16.1	34.5	20.5	11.9	16.5	2.16	-2.0	-	30.9	20.2
8	2.45	5.25	3.00	1.75	8.94	1.17	1.0	-	9.79	3.27

Table 4 *Sensitivities to variations as given in table 3 (representative of original radiometer data) and table 1 (representative of corrected data) assuming an open water surface. Algorithms are referred to by number as defined in Section 2.*

Alg. No.	clw		water vap.		Air temp.		Total	
	Orig	Corr	Orig	Corr	Orig	Corr	Orig	Corr
1	0.18	0.38	0.69	0.09	0.01	-	0.71	0.20
2	0.88	1.88	0.69	0.09	0.05	-	1.12	0.88
3	-1.05	-2.25	0.03	0.01	3.23	-	3.40	1.93
4	-1.05	-2.25	0.02	0.01	3.12	-	3.29	1.88
5	-0.88	-1.88	0.34	0.05	3.96	-	4.07	2.17
6	-0.18	-0.38	0.34	0.05	1.93	-	1.97	0.98
7	1.75	3.75	1.72	0.23	0.02	-	2.45	1.77
8	0.35	0.75	1.03	0.14	2.07	-	2.34	1.10

Table 5 *Sensitivities to variations as given in table 3 (representative of original radiometer data) and table 1 (representative of corrected data) assuming a First Year ice surface. Algorithms are referred to by number as defined in Section 2.*

Alg. No.	clw		water vap.		Air temp.		Total	
	Orig	Corr	Orig	Corr	Orig	Corr	Orig	Corr
1	-0.53	-1.13	0.69	0.09	0.01	-	0.87	0.54
2	0.88	1.88	0.69	0.09	0.05	-	1.12	0.88
3	-3.68	-7.88	0.02	0.01	3.51	-	5.09	4.08
4	-3.33	-7.13	0.34	0.05	3.95	-	5.18	3.87
5	-3.85	-8.25	0.03	0.01	3.34	-	5.10	4.20
6	-2.28	-4.88	0.02	0.01	0.87	-	2.44	2.32
7	1.75	3.75	1.72	0.23	0.02	-	2.45	1.77
8	-1.23	-2.63	1.03	0.14	1.83	-	2.43	1.54

Table 6 *Sensitivities to variations as given in table 3 (representative of original radiometer data) and table 1 (representative of corrected data) assuming a Multi Year ice surface. Algorithms are referred to by number as defined in Section 2.*

6. Evaluation study

The objective of the evaluation study is to confirm the findings from the previous section by considering actual observations over areas with stable and known surface types, if possible. In addition to this, the investigation should enable a validation of the SAF tiepoint set over ice surfaces, as the performance over open water has been shown in section 3.3. The analysis falls in two parts, first the conclusions regarding the use of the 85 GHz are examined, secondly a thorough analysis is made to examine the usefulness of the SAF tiepoints and the conclusions regarding the performance of the low frequency algorithms over sea ice areas.

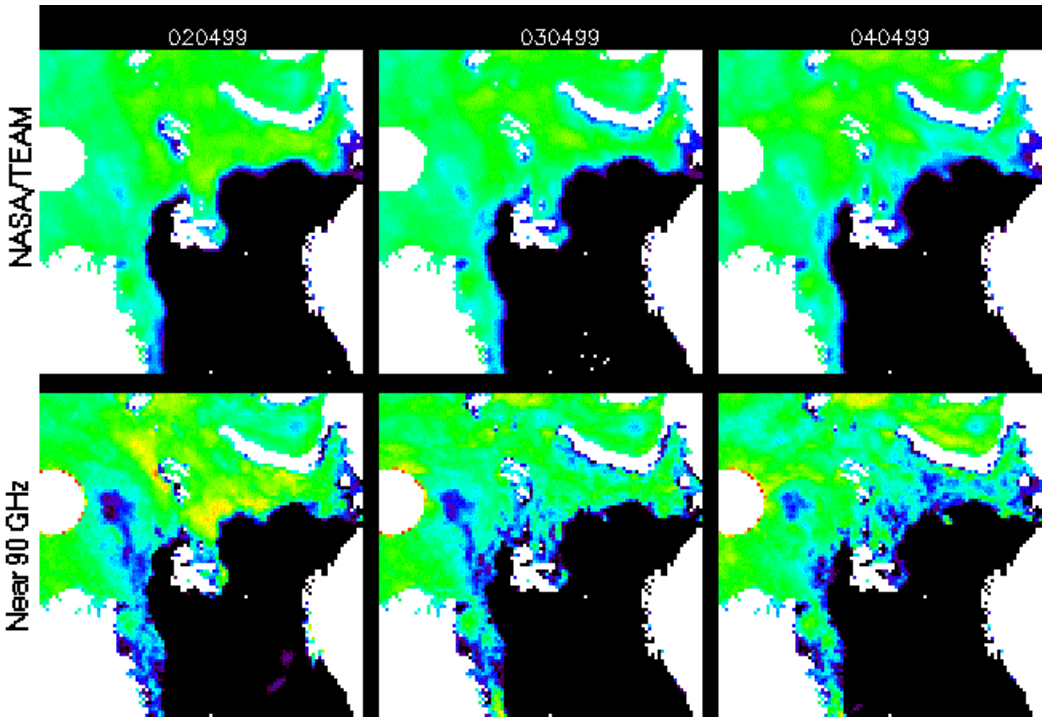

Figure 6 Timeseries of concentration retrieval using NASA/TEAM (top row) and the Near 90 GHz algorithm (bottom row). Notice the weather contamination protruding North of the Fram Strait is far more prominent in the Near 90 GHz retrievals. The colorscale is from approximately 50% (black) to 140 % (read) to highlight variations within the ice covered portion of the images.

At first, to validate the conclusions from the sensitivity study pertaining to the use of 85 GHz channels a three day timeseries of concentration retrievals using the NASA/TEAM and the Near 90 GHz algorithm is inspected, see Figure 6. As could be expected, the variations from day to day are much larger for the Near 90 GHz algorithm. Weather induced effects are expected to raise the concentration and it is evident that the yellow hues observed in the lower panels of Figure 6 vary rapidly and therefore most probably are due to passing weather contamination. Additionally, on April 2 over the open ocean off Norway the increased sensitivity to weather effects at 85 GHz results in spurious ice concentrations exceeding 50 %. Besides these obvious features, large areas show depressed concentrations varying more slowly in time. In particular a large area is apparent stretching North from the Fram Strait, weakening over time. AVHRR imagery from April 2 (Appendix C) shows high concentrations in the

area but otherwise gives no hint to the origin of this depression. One can speculate that different effects in e.g. the snow cover play a role. In particular unvalidated results seem to indicate that grain sizes in excess of 3 mm may affect the radiation at high frequencies significantly (Kern, personal communication). Another area of interest in this connection is the one East of Svalbard. Here increased concentrations are estimated by the Near 90 GHz algorithm on April 2, decreasing to quite low concentrations on April 4. This may be correlated with the temperatures at Longyearbyen, Ny Ålesund and Hopen that all display temperatures around or above freezing on April 2, returning to temperatures well below freezing on April 3 and 4. This impression is confirmed by NWP model fields of near surface temperature (Appendix C), indeed showing an intrusion of mild air on April 1 approximately coincident with the area of depressed concentration NW of Svalbard, moving Eastward to coincide with the band of high 85 GHz concentrations found on April 2 East of Svalbard. Exact knowledge of the physical processes that have taken place over the three day period are not available. However, the data above seem to suggest that the 85 GHz concentration anomalies could be explained as a combination of precipitation of large grain size snow (raising the concentration), wetness of the snow cover (raising the concentration) due to the high temperature and a subsequent rapid refreezing causing ice crusts to form inside or on the surface of the snow covered surfaces (lowering the concentration). On top of this, the temperature field of April 3 seems to suggest that to the East melting conditions prevail, so that the depressed concentration found in the Barents Sea on April 4 in both the NASA/TEAM and the 85 GHz retrievals are likely to be associated with true variations in the ice concentration. In conclusion it must be said that although the 85 GHz channels offer more detail than the low frequency channels, errors such as those shown in Figure 6 appear to be a serious shortcoming in automatic processing systems such as envisaged in the SAF. For manual interpretation, including auxiliary information, the high frequency data are excellent and able to offer much information on the structure of the sea ice cover.

Next to investigate the use of the SAF tiepoints and validate particular features found in the sensitivity analysis, the NASA/TEAM and the Comiso Frequency mode algorithms are examined in detail over areas with climatologically wellknown surface type. Due to the general circulation of the Polar Ocean, the ice North of Greenland and especially the Canadian Archipelago belongs to the oldest in the Northern hemisphere, whereas along the Coast of Siberia, there is generally ice free conditions during the summer. Consequently, study areas were chosen in these two areas, as depicted in Figure 7, to give observations of pure FY and MY ice, whereas open water samples were found in the North Atlantic South of Svalbard. These areas are believed to be representative of the given surface types during the winter season. However, at the onset of melt conditions, large variations are known to occur, spatially as well as temporally and less weight can be given to the results in those conditions.Over these areas, two years (1997 and 1998) of gridded brightness temperature data (NSIDC, 1996) was extracted and converted to ice concentration using the NASA/TEAM and Comiso Frequency mode algorithms using either the tiepoints supplied with the algorithm or the SAF tiepoints.

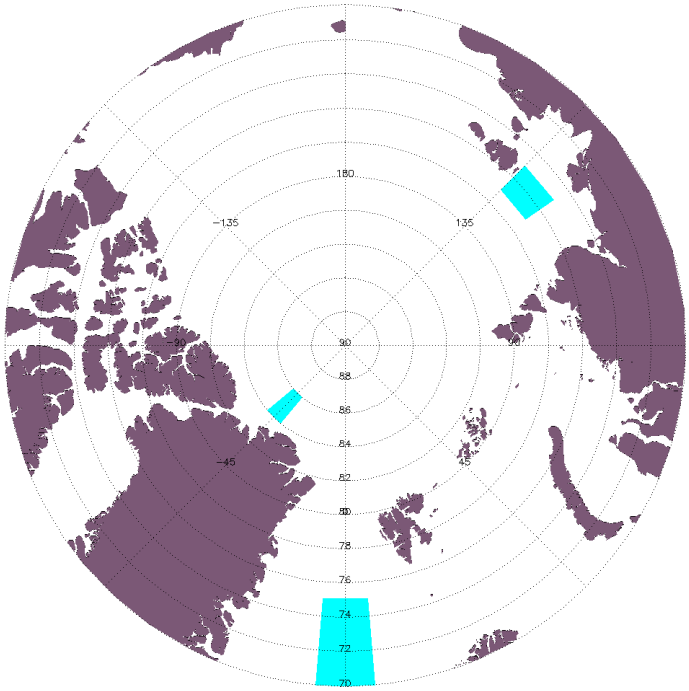

Figure 7 Definition of study areas containing pure surfaces of open water, MY and FY ice.

Over open water, as shown already in section 4, the Comiso frequency mode algorithm displayed a significantly lower noise level compared to the NASA/TEAM algorithm that in turn outperformed the Comiso polarisation mode algorithm. This behaviour exactly reflects the findings of the previous section. However, over ice covered surfaces additional sources of interference exist, due to e.g. varying surface properties and internal scattering processes within the ice. Figure 8 presents the evolution of the monthly averaged concentration time-series. During 1998, there was extensive melting in the area North of Greeland, which explains why the concentrations in Figure 8(a) are significantly depressed over the summer. Statistics are quoted for the entire dataset as well as for a dataset excluding the summer months (June-September). Comparing Figure 8(a) and (b) it is found that the NASA algorithm is significantly more stable than the Comiso Frequency mode algorithm. Over FY ice the differences are smaller. This also is in good accordance with the findings from the preceding section. In particular it is seen that by the end of the year 1998, after the extensive melt and subsequent freezeup that year the Comiso algorithm attains a higher value than the same time of previous years.

As for the significance of the tiepoints, the statistics show that, during winter the concentration series computed using the monthly SAF tiepoints is more stable than using the tiepoints supplied with the algorithms. Hence for winter conditions the tiepoints account to an extent for the climatological variations in surface emissivity. However, during summer, the original bootstrap summer tiepoints appear to deliver more stable concentration series. This is not entirely surprising, considering the method of extracting histograms over 200x200 km squares, used in the derivation of the monthly tiepoints, see Andersen (1998). During summer, the spread in surface conditions is immense and it is quite simply not possible to obtain a sufficiently clean sample of a given surface over such large areas and the histograms are therefore easily misinterpreted. The cluster analysis method, described in Comiso et al.

(1997) in that case turns out to be superior. To obtain optimum results, during summer the SAF tiepoints should therefore be substituted with the seasonal Comiso tiepoints. This should not be necessary for the NASA/TEAM algorithm, on the other hand, as results differ little with the tiepoint set used.

In light of the obvious complementary behaviours of the NASA/TEAM and the Comiso frequency mode algorithms an optimal solution for use in the SAF sea ice concentration product would appear to be a combination of the two. The NASA/TEAM algorithm should be given very little weight at low concentrations, while the opposite should be the case over high ice concentrations. The following equation is a union of these properties, gradually increasing the weighting of the NASA algorithm up to a concentration threshold T, from where it is given full weight:

$$C_T = \left(1 - W_C\right) \cdot C_{NASA} + W_c \cdot C_{Comiso}$$
$$W_C = \frac{\left|T - C_{T_0}\right| + T - C_{T_0}}{2T} \qquad (13.)$$

To avoid the need for an iterative solution, $C_{T_0} = \sqrt{C_{NASA} \cdot C_{Comiso}}$ rather than the more accurate $C_{T_0} = C_T$ can be used without incurring large errors. From the results of the sensitivity study a loose value of T between 20 and 40% would appear to make a good compromise.

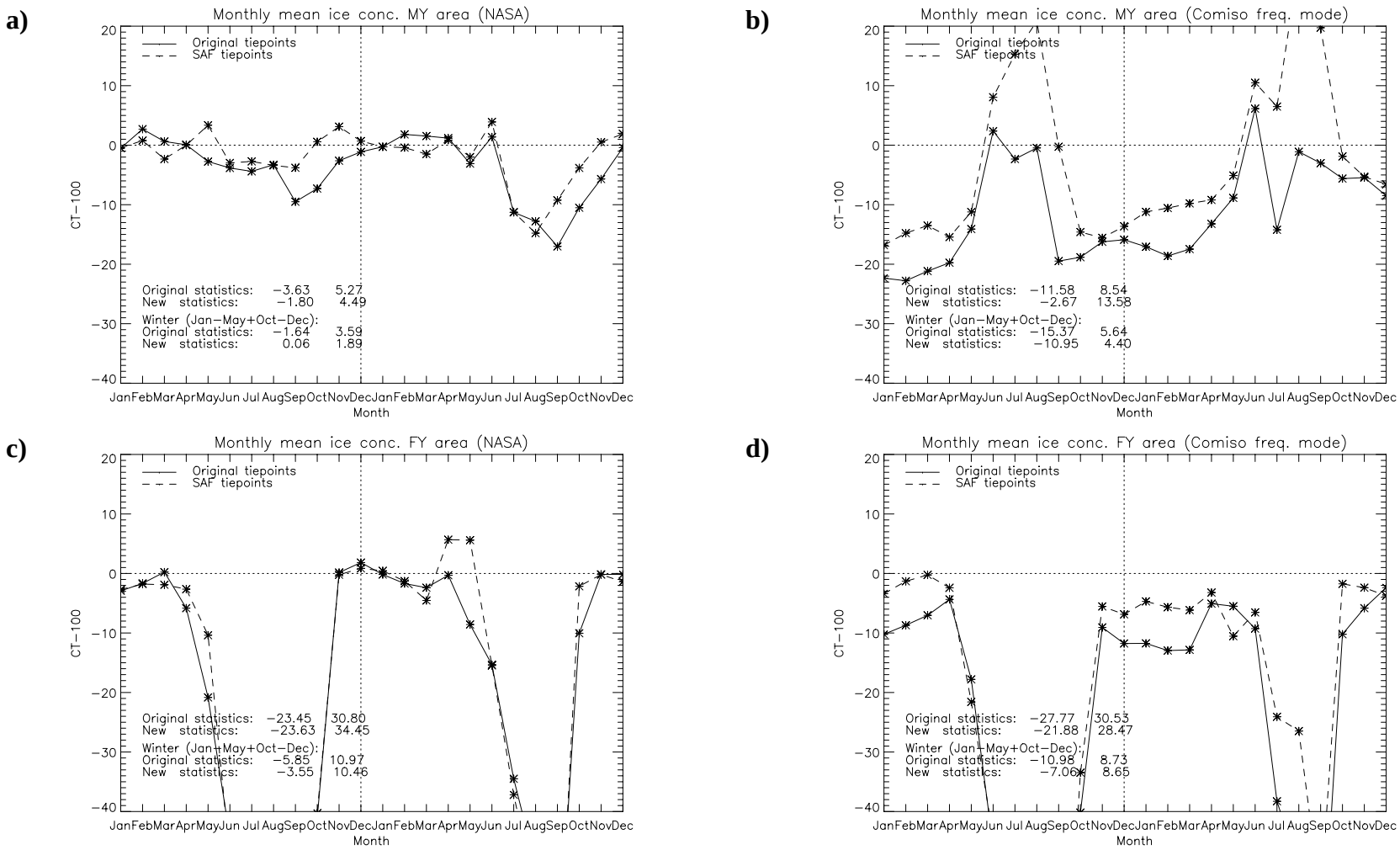

Figure 8 Monthly mean concentrations over MY (a, b) and FY (c, d) surfaces defined in Figure 7 computed using the NASA /TEAM (a,c) and the Comiso frequency mode (b,d) algorithms. Statistics (mean and standard deviation) are printed within the plots for both winter months and the entire year. Concentrations are calculated using the tiepoints supplied with the algorithms (full lines) or using the SAF monthly tiepoints (dashed). The data span the years of 1997-1998.

7. Choice of channels for multisensor products

SSM/I data is envisaged to contribute to both the ice edge and -type multisensor products. The technique of joining different datasources adopted within the present project relies on a Bayesian framework. In the simplest case of separating water from ice using one measured parameter, it can be written as

$$p(I|A) = \frac{p(A|I)}{p(A|I)p(I) + p(A|W)p(W)} \cdot p(I) \qquad (14.)$$

Where p(I|A) is the probability of there being ice given an observation A, whereas p(A|I), p(A|W) are the probabilities of making the observation A given there is ice or water respectively. The prior probabilities, p(I) and p(W), can be set to 50% in the case where no prior knowledge or assumptions are available and cancel out. The formula can easily be extended to cover additional observation- and surface types under the assumption that the observations are independent. In the following the suggestions and rationale for selection of suitable SSM/I parameters for both ice edge and type will be given.

7.1 Ice type

In ice type determination the difference in the level of radiation emitted by the different surfaces could be used. However using the level alone introduces a dependence on surface temperature, that can introduce uncertainties. A more robust parameter is the Gradient Ratio computed as in equation 1. This parameter reflects the slope of the brightness temperature as a function of frequency. For open water it will be positive, for MY ice it will be negative while for FY ice it will be close to 0. The gradient ratio can of course be computed between any pair of frequencies. Andersen (1998) found anomalous behaviour of the GR(37,85,V) field for extended periods during the ice season 1996-1997, whereas the GR(19,37,V) remained stable. There is hardly any other parameter than GR, that is equally efficient for ice type detection and considering the above it seems sensible to adopt the GR(19,37,V) as the passive microwave parameter to enter the ice type determination. It should be noted, however, that in a mixture of MY ice and open water, the GR signature will resemble FY ice. Therefore a correction for ice concentration should be applied, such that only the gradient ratio of the ice covered portion of the pixel is taken into account. Assuming the brightness temperature measured by the radiometer is a linear mixture of the emissions of the water and ice portion of a given pixel the brightness temperature of the ice covered portion of the pixel can be calculated as:

$$T_{B,I} = \frac{T_B - (1 - C_T)T_{B,W}}{C_T} \qquad (15.)$$

where C_T is the total concentration e.g. from the SAF concentration retrieval, T_B is the observed brightness temperature and $T_{B,W}$ is the open water tiepoint brightness temperature. It is the gradient ratio computed from $T_{B,I}$ that should be used in the ice type analysis. Over consolidated ice, $T_{B,I}$ will be equivalent to the observed brightness temperature and the gradient ratio will be unchanged.

7.2 Ice edge

In the selection of the SSM/I parameters to enter the multi-sensor ice edge calculation, the choice is larger and it is useful to first consider the nature of the problem. The objective is to determine suitable observed parameter(s) that give the maximum amount of independent information and subsequently to parameterize the probability distributions p(A|I) and p(A|W). Over open water, the brightness temperatures grows with atmospheric water content and surface wind. This means that there is a lower bound but no welldefined higher bound on the brightness temperature. Over an ice covered surface, including the marginal ice, the brightness temperature essentially grows with increasing ice concentration and is bounded by the 0 and 100 % concentration limits. Thus, for the case of both water and ice, one would expect probability distributions with a relatively long tail on one side.

There is a vast amount of different parameters that could potentially be of use, however they can be divided into the following 4 classes: polarisation ratios, gradient ratios, linear combinations and concentration retrievals. The last two classes to some extent overlap, in that most ice concentration algorithms are linear functions of brightness temperatures, the difference would be the use of variable tiepoints in the concentration algorithms. The virtue of the two types of ratios is that they vary little with surface temperature and therefore remain relatively constant throughout the year. The gradient ratios on the other hand are less convenient for use in the ice edge product due to their bimodal nature over ice introduced by the sensitivity to ice type. The polarisation ratios display well defined peaks over ice as well as over water and vary monotonically with ice concentration as well as with the atmospheric contributions. When it comes to concentration estimates or linear combinations of brightness temperature, the concentration estimates are preferable due to their suppression of different noise sources and seasonal variations. This means that the central value of the distributions remains nearly the same over the year, however the width and perhaps even shape of the distributions will vary with the increased variability in ice surface and atmospheric properties. For the separation of water from ice, the most important aspect is to ensure as narrow a distribution of the probability given water as possible. In that respect, the Comiso Bootstrap algorithm offers the sharpest separation of the algorithms studied here. The uncertainty linked with the sensitivity to cloud liquid water over consolidated MY ice is an issue when ice concentration retrieval is concerned but is unlikely to affect the accuracy of the much more robust problem of separating ice from water. Having established the low resolution/low noise input to the integration scheme, it is desirable to add high resolution information from the 85 GHz channels. In that case, the only attractive candidate is the 85 GHz polarisation ratio, PR(85).

The final and very important issue is to establish the parameterisation of the probability distribution functions (PDFs) to be used. Figure 9 displays in more detail the histograms of PR_{85} and ice concentration computed using the Comiso Frequency mode algorithm. Shown in dashed style, the corresponding histogram after masking out possible ice infested areas is shown. In particular the concentration histograms show pronounced tails and thereby strengthen the physical reasoning above. The polarisation histogram on the other hand is hardly skewed and therefore a gaussian distribution as used in earlier work will be sufficient (Breivik et al., 1999). As for the PDF over ice, sofar a collocation of navigational ice charts

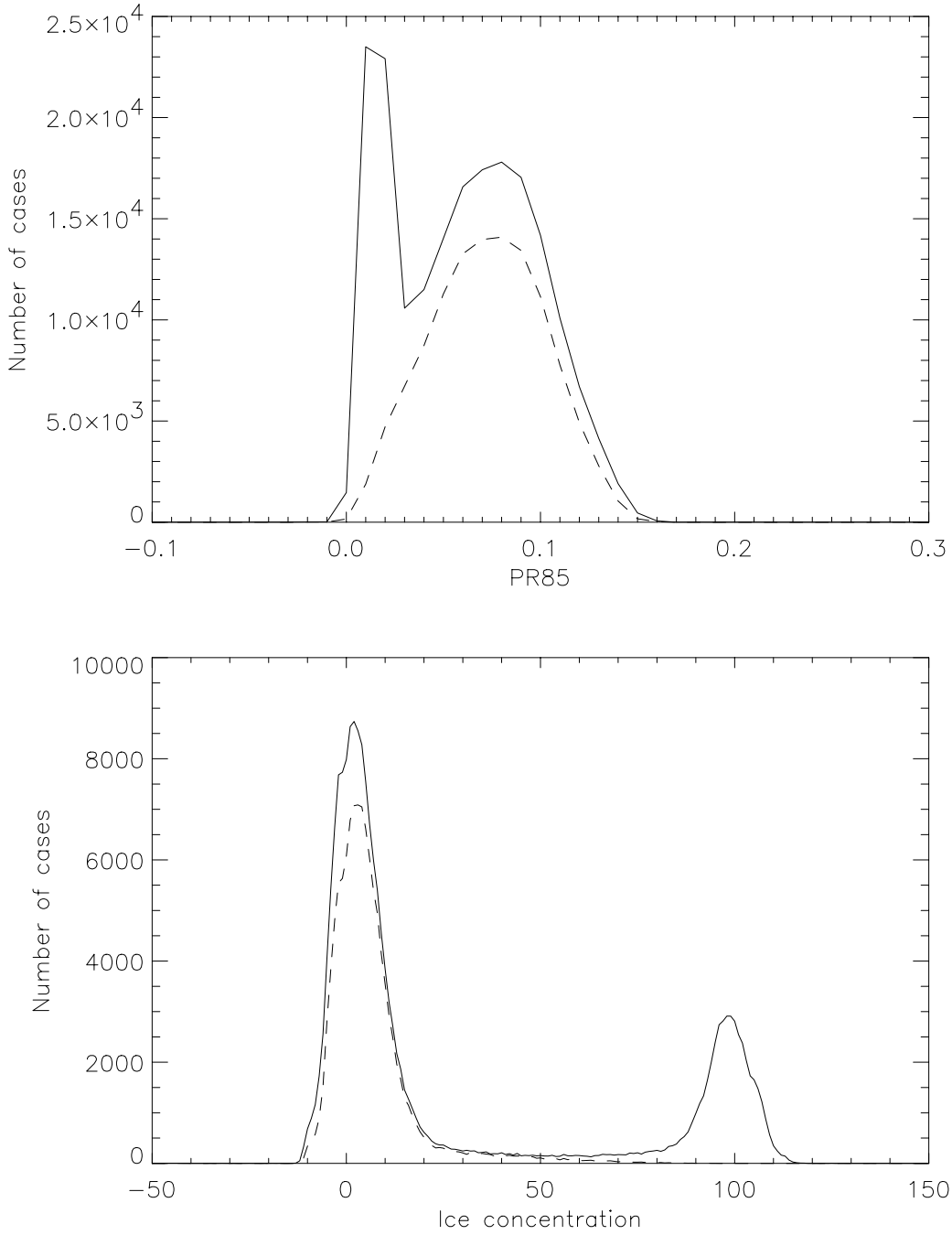

Figure 9 Histograms of polarisation ratio 85 GHz (top) and ice concentration from the Comiso Frequency mode algorithm (bottom) based on 10 days of SSM/I data during Jan 1996. Dashed lines show the histogram when ice has been masked out.

and observed data has been used and gaussian PDFs have been derived for different concentration intervals. These PDFs are symmetric around the central value as no physical process provides a directional influence.

To describe the PDF of the concentration estimates over water that display the observed tails include the generalised gamma distribution (Stacy and Mihram, 1965):

$$g(x;a,h,A) = \frac{h}{\Gamma(a)\cdot A}\cdot\left(\frac{x}{A}\right)^{ah-1}\cdot\exp\left(-\left(\frac{x}{A}\right)^{h}\right) \qquad (16.)$$

The n'th moment of the distribution is given as:

$$M_n = A^n\frac{\Gamma\left(a+\frac{n}{h}\right)}{\Gamma(a)} \qquad a+\frac{n}{h}>0 \qquad (17.)$$

After offsetting the data and imposing a lower limit such that no negative data values exist it is possible to solve for the parameters a, h and A using the method of Stacy and Mihram (1965). However, difficulties arise from the dependence on the empirical skewness coefficient, that is difficult to estimate in a sufficiently stable manner. Subsequently trials were made with the special cases where a=1 (Weibull distribution) and h=1 (two parameter gamma distribution) and it was found that the gamma distribution is best describing the data. In appendix B, monthly results are given based on Comiso frequency mode ice retrievals computed from both atmospherically corrected and raw brigtness temperatures. It is evident that both standard deviation and bias of the concentration estimates benefit from the NWP based atmospheric correction procedure. However, it is more difficult to fit the gamma distribution to the corrected concentration histograms and the rapid decline of the tail is not matched exactly. In spite of this difficulty, the PDFs approach zero at a 5-10% lower concentration value when compared to the use of uncorrected brightness temperatures, which is equivalent to a better detection of the low concentration portion of the marginal ice in the multisensor ice edge analysis. As for the seasonal variation of the PDFs, the worst fits and widest distributions are found during the summer months and therefore a lower performance must be expected during these months. It is possible to use the work of Kern (1999) to correct also the 85 GHz SSM/I channels, however the efficiency is limited by the fact that the 85 GHz radiative transfer is far more sensitive to atmospheric liquid water content, which has been shown to be very difficult to deal with. However, in any case the quality is improved using corrections for water vapour and wind.

8. Conclusions and recommendations

The criteria for selecting the final sea ice concentration algorithm include the following:

1. Accuracy of concentration estimate
2. Noise resistance
3. Resolution

Of these the last point is to a large extent in contradiction to the first two. However, as the SAF targets a wide community with differing knowledge of sea ice analysis and to a wide extent will be a source of data to automatic processing, it seems important to provide a robust product. Therefore the emphasis has been given to the first two points, ruling out the use of 85 GHz that provides higher resolution at the expense of higher noise levels. Based on both model and observed data, it is found that NASA/TEAM and the Comiso Frequency mode algorithms are least sensitive to geophysical noise. A complementary behaviour has been found between the algorithms, such that the Comiso algorithm displays stable retrievals over open water and low ice concentrations, whereas the NASA/TEAM algorithm is insensitive to noise over consolidated ice. To profit from this complementarity a smooth combination of the NASA/TEAM algorithm and the Comiso frequency mode algorithm is envisaged. There are many options for combining the two algorithm estimates, however it is important that the virtues of each algorithm be retained. This means that the NASA/TEAM algorithm should be given very little weight at low concentrations, while the opposite should be the case over high ice concentrations. A weighting scheme is suggested to accomplish this.

As for the seasonal stability of the concentration retrieval it is shown that the use of monthly tiepoints raises the performance over sea ice in all cases except for the Comiso algorithm during the summer months. This is due to difficulties in the procedure used to establish the monthly tiepoints (Andersen, 1998). It is therefore recommended to use the Comiso summer tiepoints (Comiso et al., 1997) in this period.

Use of threshold based weather filters such as that of Cavalieri et al. (1995) is found to very efficiently mask out spurious ice, although it can occasionaly saturate and even trigger within the ice pack. Further, at the ice edge it is shown that the use of thresholding is not able to correct partially weather contaminated pixels, i.e. pixels with less than 100% true concentration and weather contamination. At this point both the correction method of Thomas (1998) and a method using NWP model fields are considered. The former method uses extrapolation of retrieved atmospheric fields over the marginal ice, which may introduce artefacts, whereas errors in the NWP model fields results in suboptimal performance for the latter method. The choice of method will depend on the outcome of analyses to take place in connection with the upcoming analysis of the comprehensive set of validation data being collected in the frame of the SAF project. In passing it should be noted that the NWP based method has great potential for improvement as evolving methods of data assimilation improve the NWP model analyses and forecasts.

As for the use of passive microwave data in the multisensor ice edge product, the Comiso Frequency mode algorithm retrievals and 85 GHz polarisation ratio seem to offer a good combination the former providing good stability and the latter providing high resolution. It is found that the concentration retrievals are reasonably well described by a 2 parameter gamma distribution. Monthly distributions are derived for both corrected and uncorrected brightness

temperatures and it is found that the use of the NWP based correction method results in narrower distributions. The distribution of the 85 GHz polarisation ratio on the other hand is close to a gaussian distribution.

Acknowledgements

The author gratefully acknowledges the assistance and useful discussions extended by Rashpal S. Gill, Stefan Kern and Leif Toudal Pedersen.

9. References

Andersen, S.: Monthly arctic sea ice signatures for use in passive microwave algorithms, DMI Technical Report 98-18, 1998.

Breivik, L.A.; Godøy, Ø.; Schyberg, H.; Andersen, S.: Status of the development of a multi sensor ice product. Proceedings 1999 EUMETSAT Meteorological Satellite Data Users Conference Copenhagen 6-10 September 1999.

Cavalieri, D.J; Gloersen, P.: Determination of sea ice parameters with the NIMBUS 7 SMMR. J. Geophys. Res., 89, D4, 5355-5369, 1984.

Cavalieri, D.J.: A microwave technique for mapping thin sea ice. J. Geophys. Res., 99, C6, 12561-12572, 1994.

Cavalieri, D.J.; St. Germain, K.M.; Swift, C.T.: Reduction of weather effects in the calculation of sea-ice concentration with the DMSP SSM/I. J. Glaciol., 41, 455-464, 1995.

Comiso, J.C.: Characteristics of arctic winter sea ice from satellite multispectral microwave observations. J. Geophys. Res., 91, C1, 975-994,1986.

Comiso, J.C.; Cavalieri, D.J.; Parkinson, C.L.; Gloersen, P.: Passive microwave algorithms for sea ice concentration: A comparison of two techniques. Remote Sens. Environ., 60, 357-384, 1997.

Fuhrhop, R.: MWMOD user manual, Institut für Meereskunde, Christian-Albrechts Universität, Kiel, Germany, 82 pp, 1997.

Grumbine, R.W.: Automated passive microwave sea ice concentration analysis at NCEP. Technical Note, OMB Contribution 120, National Oceanic and Atmospheric Administration, 1996.

Karstens, U.; Simmer, C.; Ruprecht, E.: Remote sensing of cloud liquid water. Meteorol. And Atmos. Phys., 54, 157-171, 1994.

Kern, S.: Compensating for atmospheric effects on passive radiometry at 85.5 GHz using a radiative transfer model and NWP model data (Report on visiting scientist stay). Institute of Environmental Physics, University of Bremen, Germany, 9pp, 1999.

Lo, R.C.: A comprehensive description of the emission sensor microwave imager SSM/I environmental parameter extraction algorithm. NRL Memo. Rep. 5199, 1983.

National Snow and Ice Data Center: DMSP F13 SSM/I Brightness Temperature Grids for the Polar Regions, Vol 1. Digital data available from nsidc@kryos.colorado.edu. Boulder, Colorado: NSIDC Distributed Active Archive Center, University of Colorado at Boulder, 1996.

Pedersen, L.T.: Retrieval of sea ice concentration by means of microwave radiometry. PhD Dissertation, Technical University of Denmark, Copenhagen, 1991.

Pedersen, L.T.: Chapter 6.2 in Sandven et al.: IMSI report no. 8. Development of new satellite ice data products. NERSC Technical Report no. 145, Nansen Environmental and Remote Sensing Center, 1998.

Ramseier R.O.: Sea ice validation. in J.P. Hollinger (ed): DMSP special sensor microwave/imager calibration/validation - Final report volume II, Naval Research Laboratory, Washington, DC, 1991.

Sass, B.H.; Nielsen, N.W.; Jørgensen, J.U.; Amstrup, B.: The operational DMI-HIRLAM system, 2nd rev. ed. DMI Technical Report 99-21, Danish Meteorological Institute, 1999.

Schrader, M.: Ein dreiskalenmodell zur berechnung der reflektivität der ozeanoberfläche im mikrowellenbereich. Technical report, Berichte aus dem Institut für Meereskunde and der Christian-Albrechts-Universität, 274, Kiel, 1995.

Simmer, C.: Satellitenfernerkundung hydrologischer Parameter der Atmosphäre mit Mikrowellen. Verlag Dr. Kovac, Hamburg, 1994.

Smith, D.M.; Barrett, E.C; Durbin, C.; Scott, J.C: Extraction of sea ice concentration from SSM/I data. Proceedings Meteorological satellite data users' conference, Winchester UK, EUMETSAT, 57-64, 1995.

Smith, D.M.: Extraction of winter sea-ice concentration in the Greenland and Barents Seas from SSM/I data. Int. J. Remote Sensing, vol.. 17, no. 13, 2625-2646, 1996.

Svendsen, E.; Kloster, K.; Farelly, B.; Johannesen, O.M.; Johannesen, J.A.; Campbell, W.J.; Gloersen, P.; Cavalieri, D.J.; Mätzler, C.: Norwegian remote sensing experiment: Evaluation of the Nimbus 7 scanning multichannel microwave radiometer for sea ice research. J. Geophys Res., 88, C5, 2781-2791, 1983.

Svendsen, E.; Mätzler, C.; Grenfell, T.C.: A model for retrieving total sea ice concentration from spaceborne dual-polarized passive microwave instrument operating near 90 GHz. Int. J. Remote Sensing, 8, 10, 1479-1487, 1987.

Thomas, C.: Langzeitanalyse der antarktischen Meereisbedeckung aus passiven Mikrowellendaten. PhD dissertation, Institute of Environmental Physics, University of Bremen, 1998.

Ulaby, F.T; Moore, R.K.; Fung, A.K.: Microwave Remote Sensing, Artech House, 1981.

Wentz, F. J.: A well-calibrated ocean algorithm for SSM/I. J. Geophys. Res., 102, C4, pp. 8703-8718, 1997.

Appendix A: Algorithm sensitivities

In the following, sensitivities of the concentration algorithms under consideration are given. The sensitivities to cloud liquid water and total water vapour are made with ice concentration varying between 0 and 100% in steps of 20 % concentration. Three such experiments are made:

1) with ice emissivity equivalent to FY ice and a temperature of the emitting ice layer of 268 K,
2) as 1 but with emissivity equivalent to MY ice and
3) as 1 but with a temperature of the emitting ice layer of 264K.

Plots of the sensitivities are found on the following pages with reference to the numbering above. Finally the sensitivity to wind over an open water surface is given on the last plot of this appendix.

Sensitivity to Total water vapour, case 1

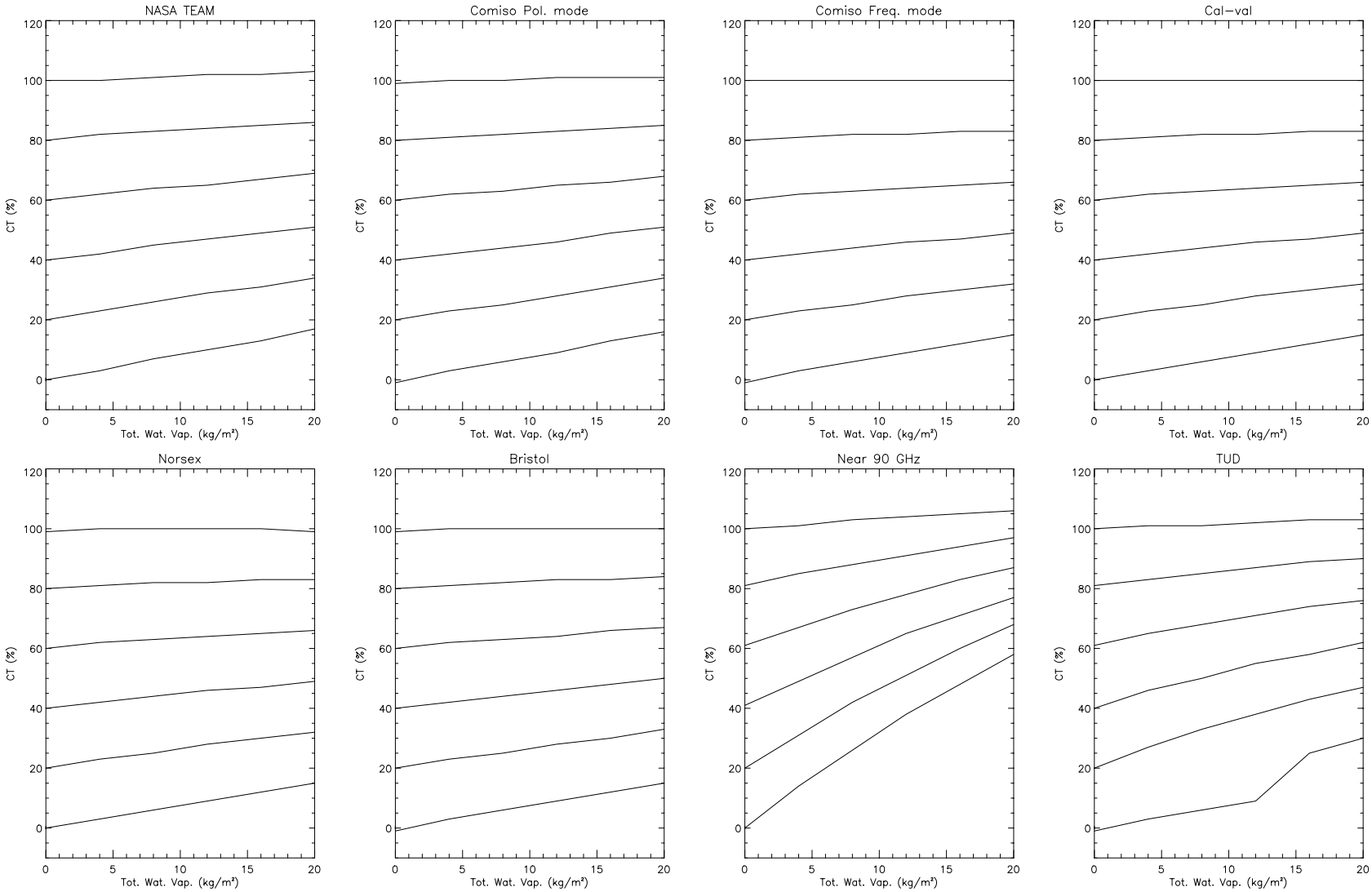

Sensitivity to Total water vapour, case 2

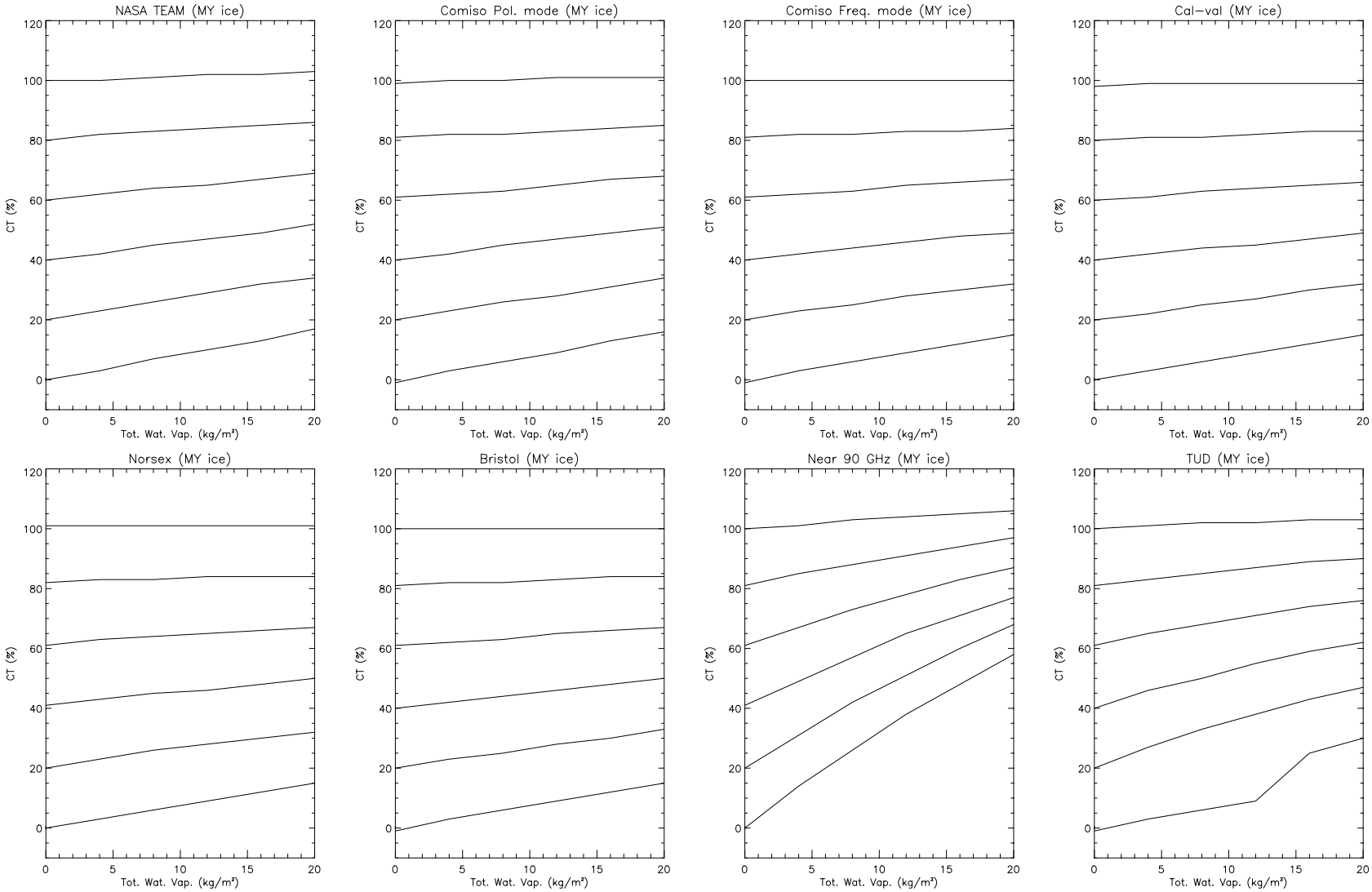

Sensitivity to Total water vapour, case 3

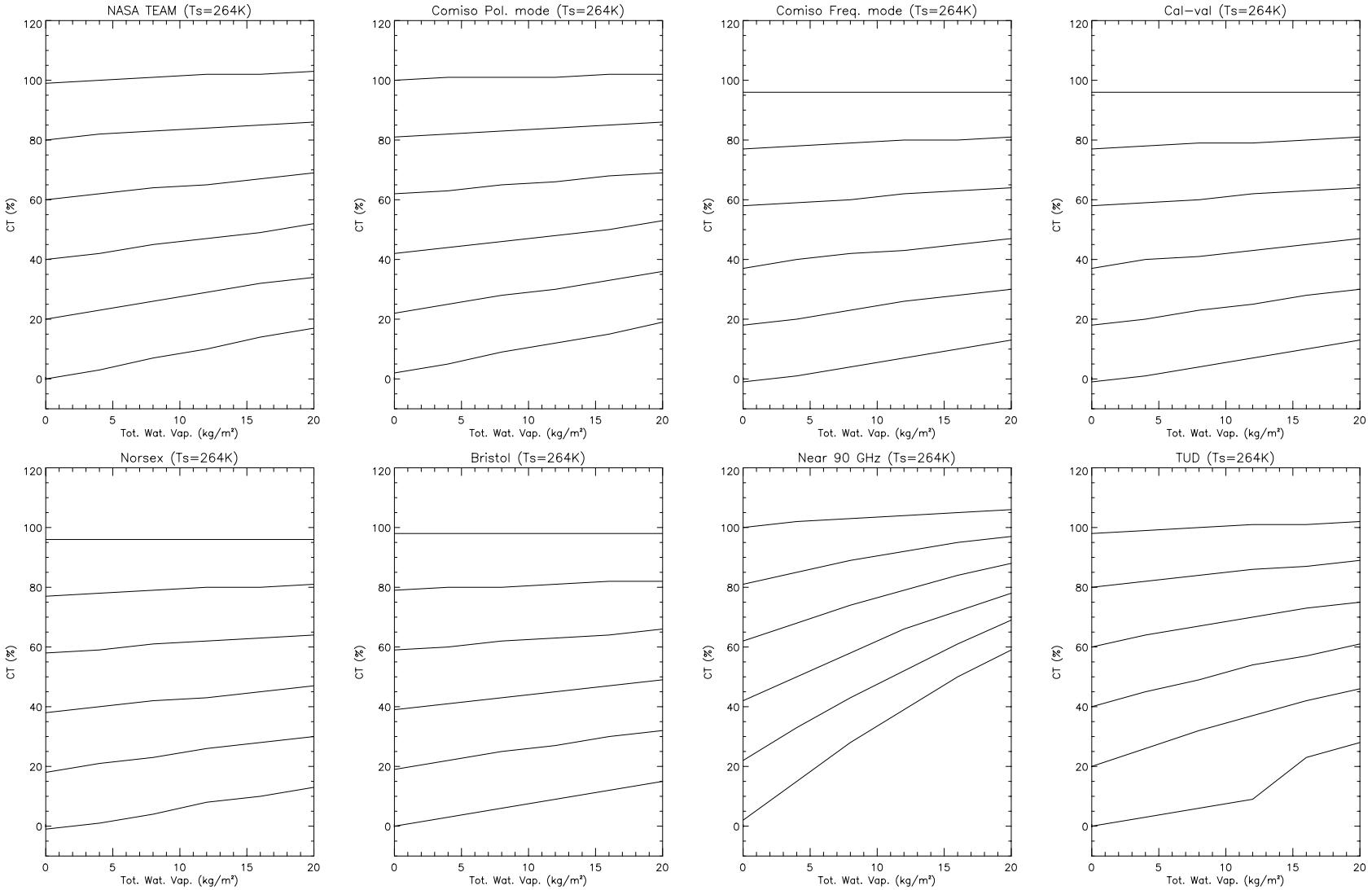

Sensitivity to cloud liquid water, case 1

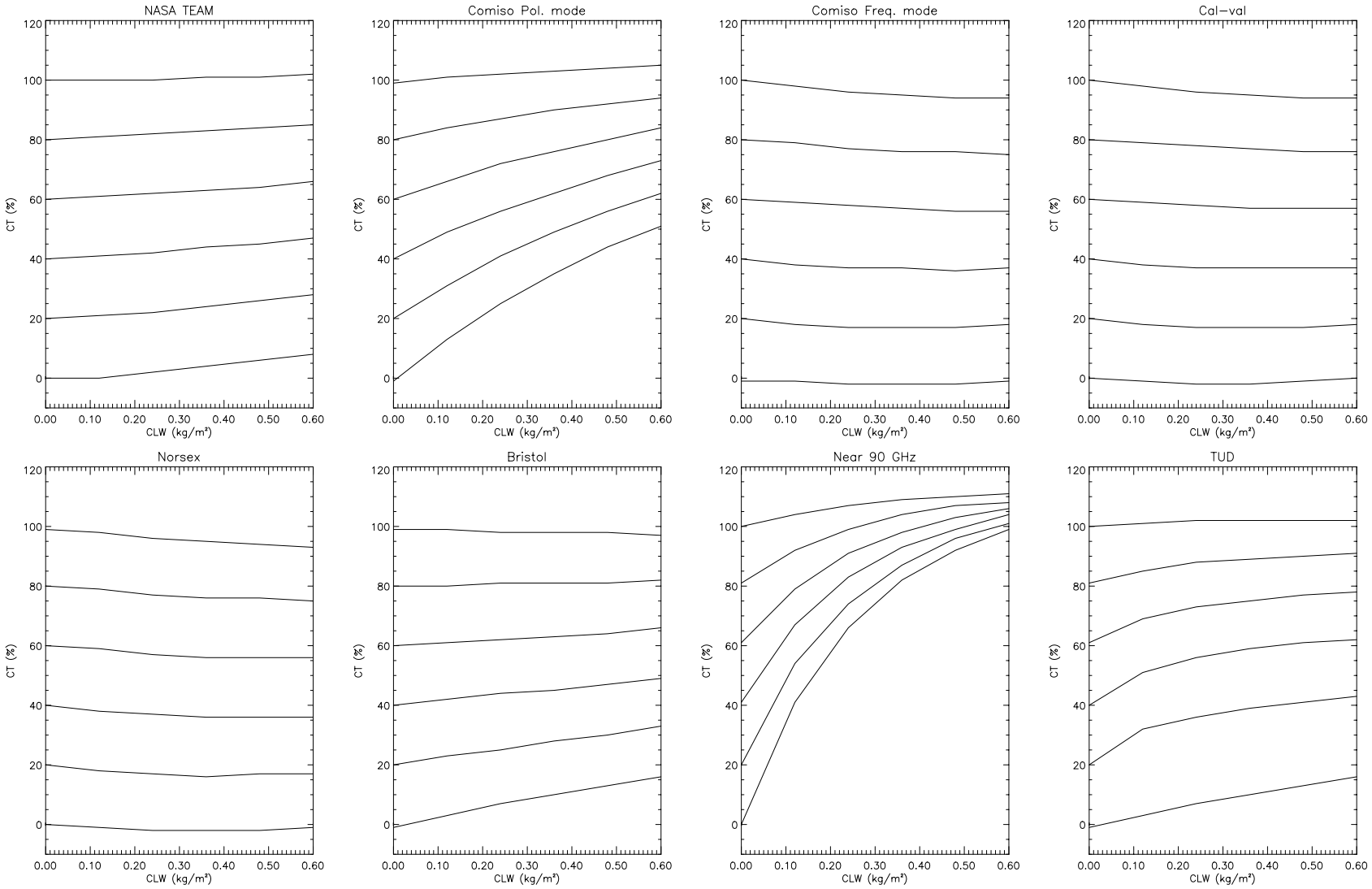

Sensitivity to cloud liquid water, case 2

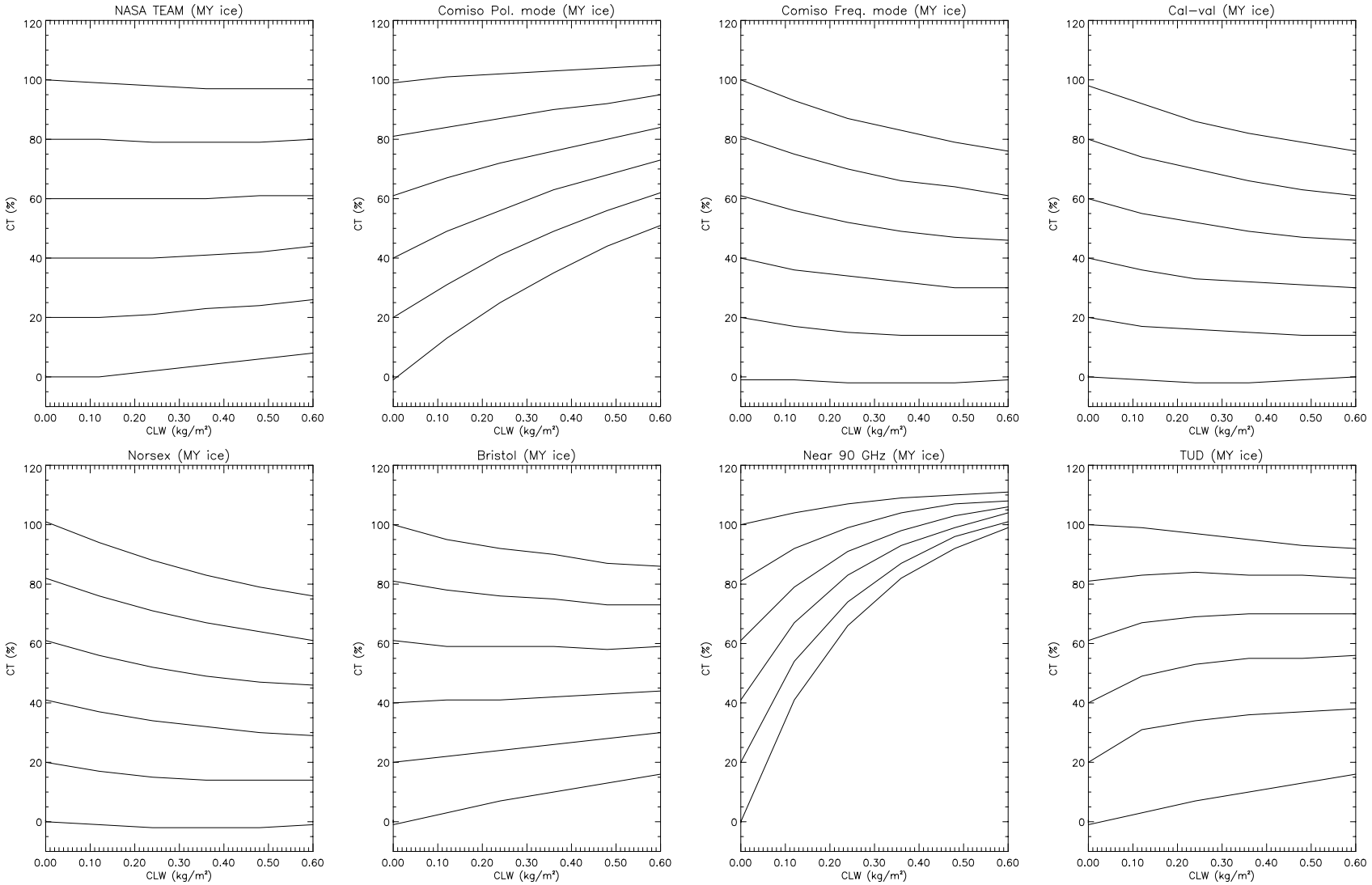

Sensitivity to cloud liquid water, case 3

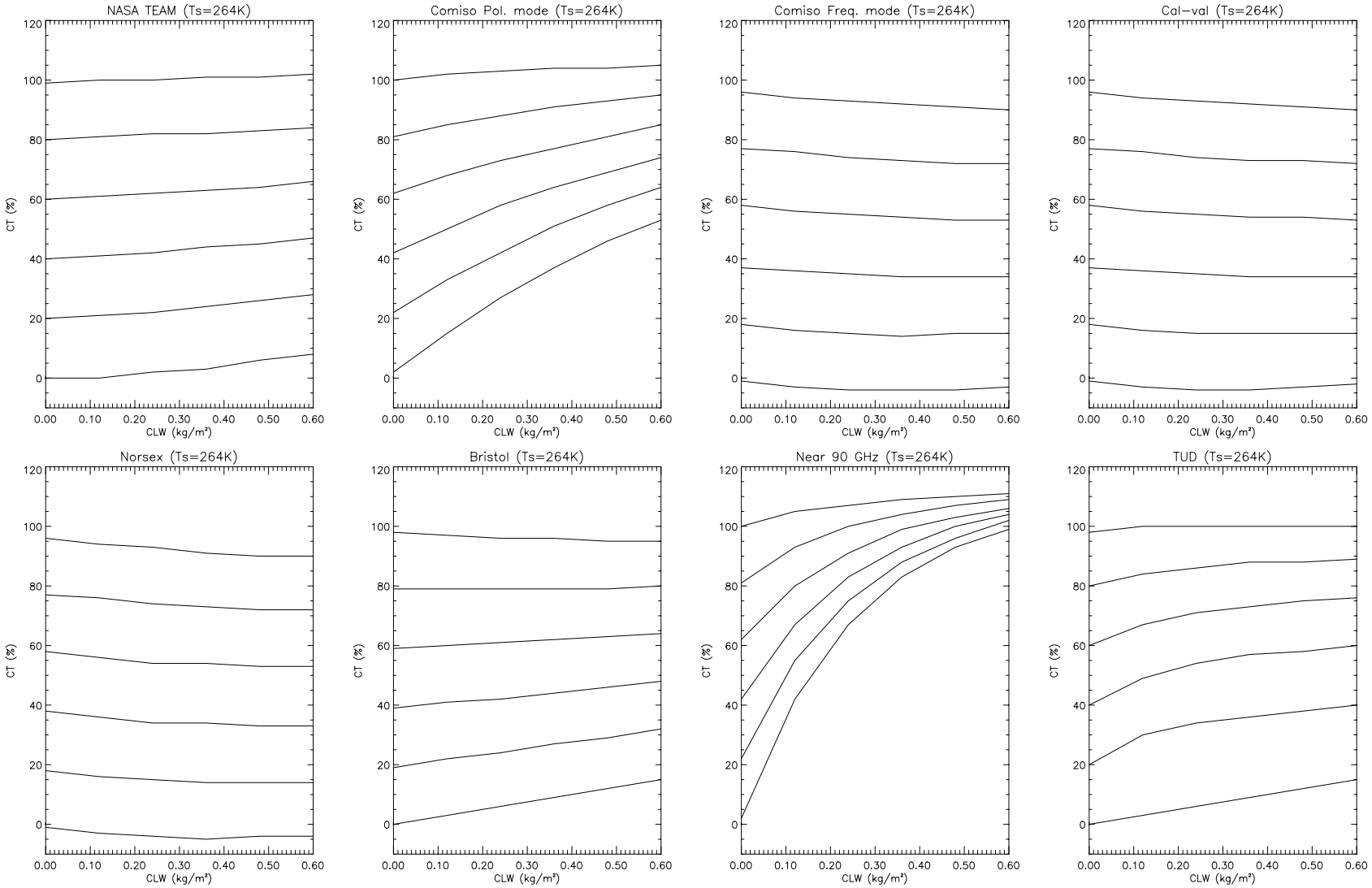

Sensitivity to wind

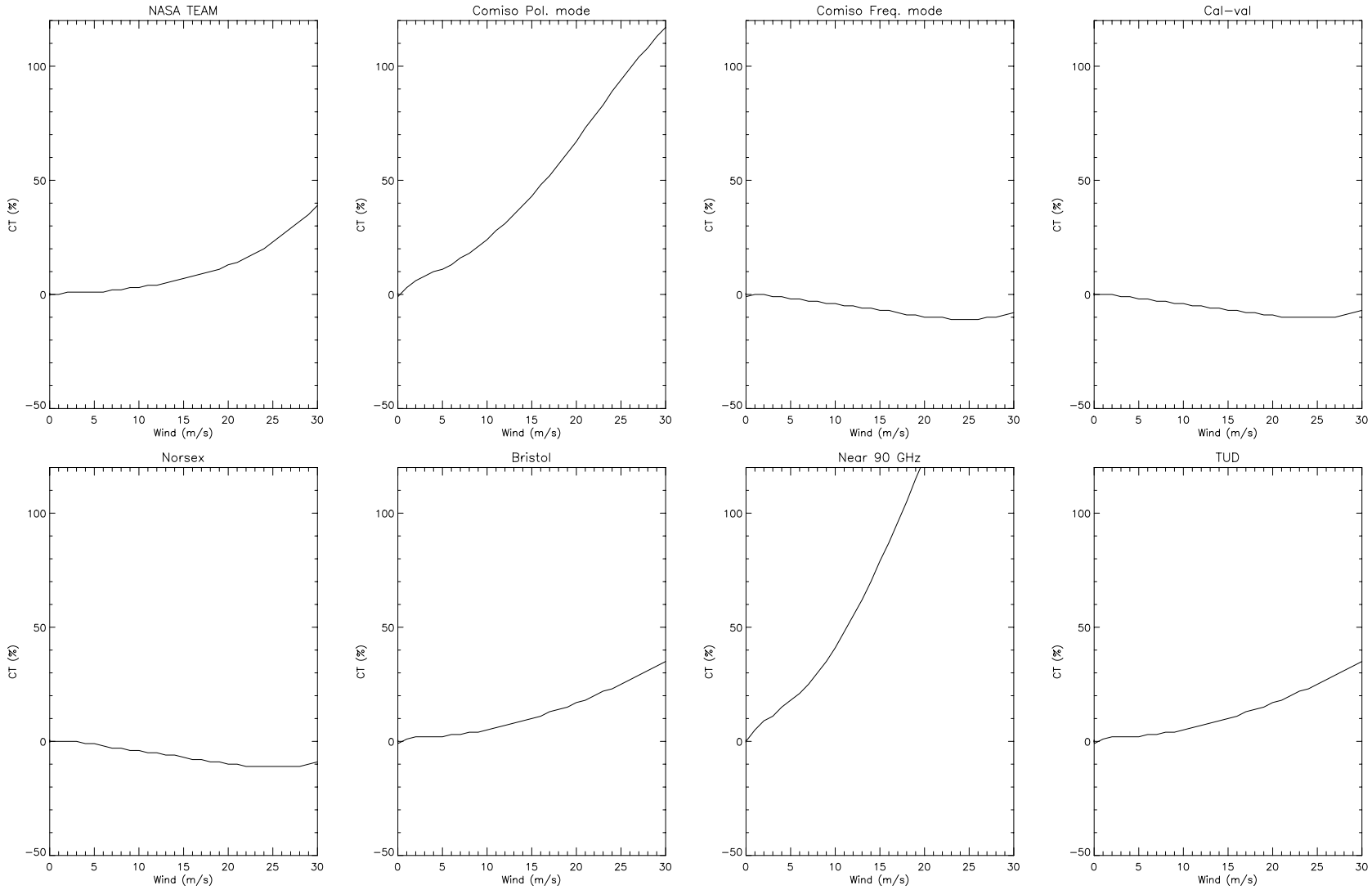

Appendix B: Ice concentration PDFs

The following distributions have been established based on concentration retrievals using the Comiso frequency mode algorithm. Values of pertinent parameters are given in the tables below, while plots of the distributions are given on the following pages. The signifcance of Kolmogorov-Smirnov tests is given for the hypotheses that a gamma and a gaussian distribution explains the data, respectively. It is seen that for the uncorrected dataset, the gamma distribution is a very good choice. For the corrected dataset, supposedly due to reduction of the tails of the observed distribution, the gaussian distribution gains better scores, while the gamma distribution scores less and more variable than for the uncorrected data .However, still the gamma distribution represents the data far better than a gaussian.

Based on uncorrected brightness temperatures:

Month	Offset	a	A	Mean	Std. dev.	Skew	KS-test (gamma)	KS-test (gaussian)
Jan	15	4,33	2,87	5,31	5,97	2,25	1,000	0,001
Feb	15	4,82	2,41	4,53	5,30	1,94	1,000	0,001
Mar	15	5,57	1,67	2,21	3,95	2,46	0,994	0,001
Apr	15	5,62	2,40	4,37	5,69	2,38	0,951	0,000
May	15	5,21	2,22	3,45	5,06	2,74	0,938	0,000
Jun	15	4,50	3,09	2,80	6,56	2,20	0,996	0,000
Jul	15	3,52	4,44	7,50	8,32	2,70	0,702	0,000
Aug	15	3,05	5,00	7,08	8,70	2,40	0,871	0,000
Sep	15	2,88	5,00	5,34	8,50	2,56	0,772	0,000
Oct	15	4,28	3,53	5,03	7,31	2,45	0,939	0,000
Nov	15	3,75	3,78	6,07	7,33	1,97	0,998	0,000
Dec	15	3,35	3,42	4,37	6,27	1,98	0,998	0,000

Based on atmospherically corrected brightness temperatures:

Month	Offset	a	A	Mean	Std. dev.	Skew	KS-test (gamma)	KS-test (gaussian)
Jan	15	3,88	2,70	-3,62	5,32	4,40	0,522	0,116
Feb	15	4,75	2,07	-4,29	4,50	3,66	0,801	0,065
Mar	15	9,71	1,08	-3,60	3,37	3,97	0,921	0,084
Apr	15	5,85	1,92	-2,90	4,63	4,88	0,309	0,065
May	15	3,92	2,50	-4,34	4,94	3,78	0,801	0,079
Jun	20	3,36	3,52	-7,26	6,46	2,94	0,869	0,009
Jul	20	2,99	4,65	-5,22	8,04	3,60	0,218	0,001
Aug	25	5,98	3,11	-5,48	7,61	4,22	0,147	0,012
Sep	25	5,06	3,64	-5,66	8,18	3,52	0,229	0,026
Oct	25	7,89	2,49	-4,41	7,00	3,32	0,396	0,015
Nov	20	6,44	2,56	-2,65	6,49	3,62	0,162	0,019
Dec	15	5,23	2,13	-3,99	4,86	3,61	0,575	0,062

Plots of concentration PDFs based on uncorrected brightness temperatures:
Full line: Observed histogram. Dashed line: Gamma PDF

Jan

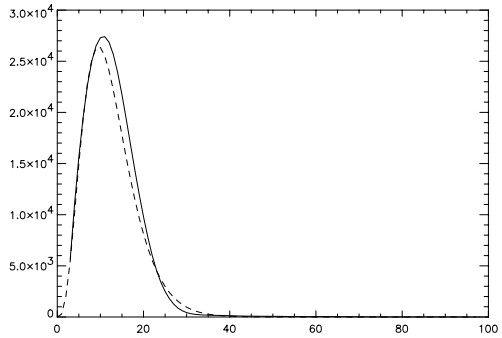

Feb

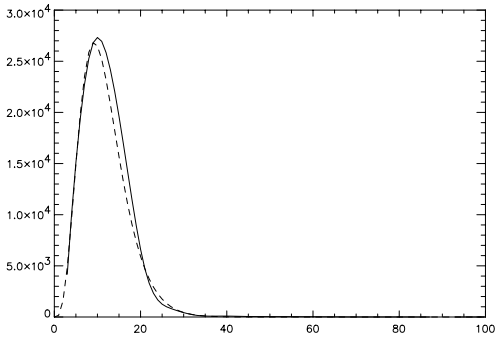

Mar

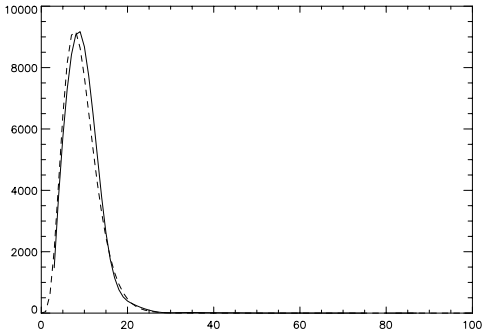

Apr

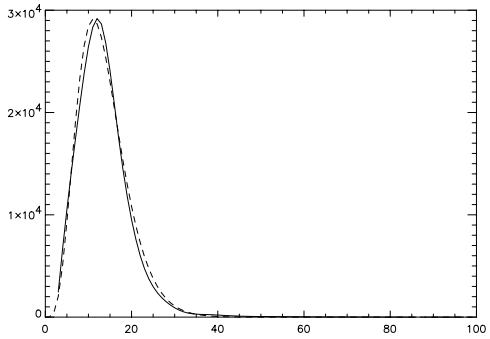

May

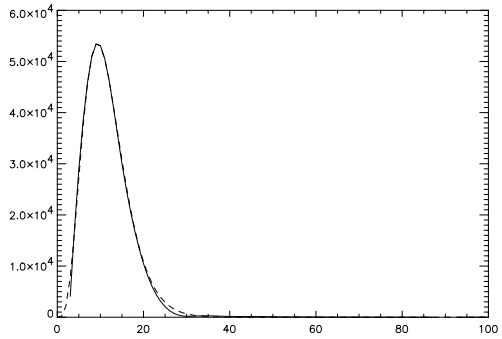

Jun

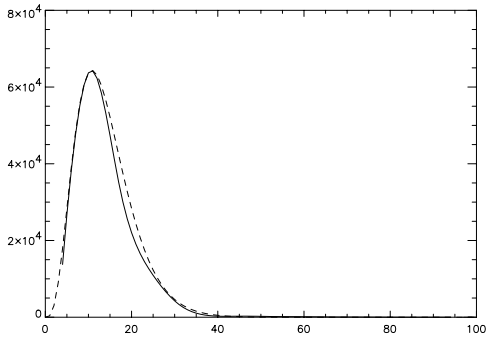

Jul

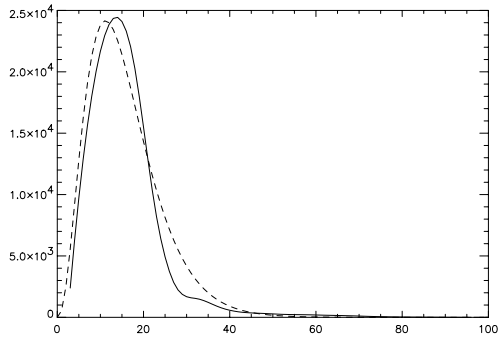

Aug

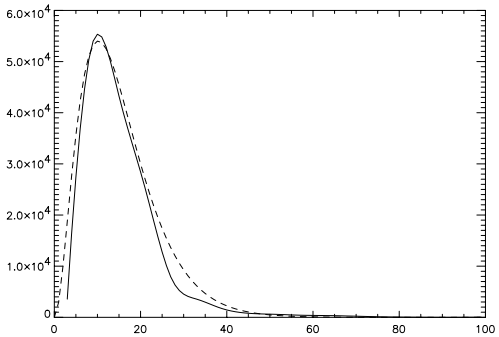

Sep

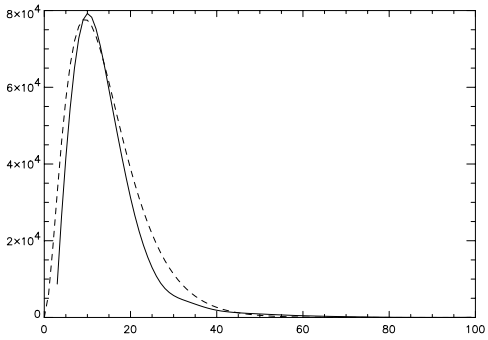

Oct

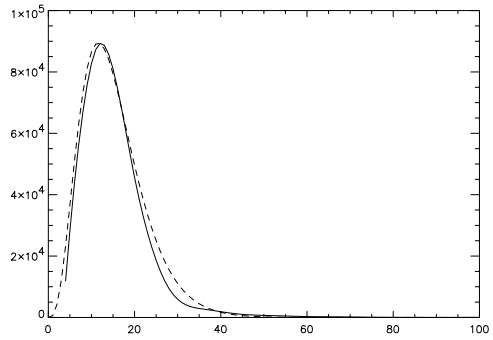

Nov

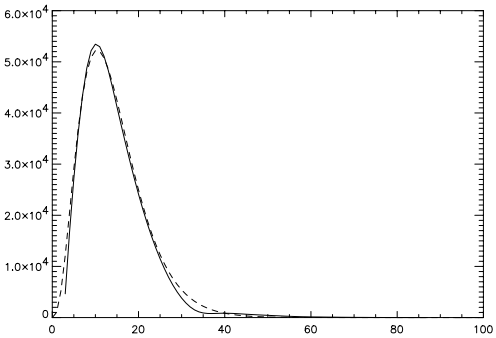

Dec

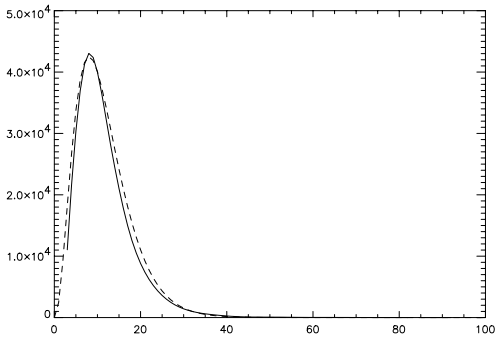

Plots of concentration PDFs based on corrected brightness temperatures:
Full line: Observed histogram. Dashed line: Gamma PDF

Jan

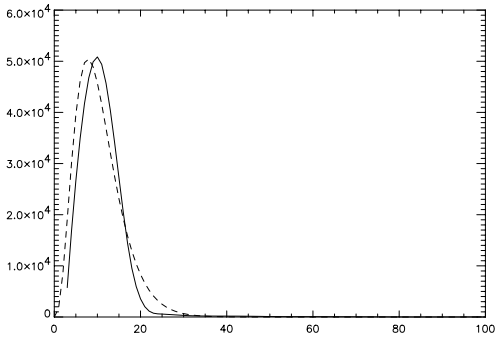

Feb

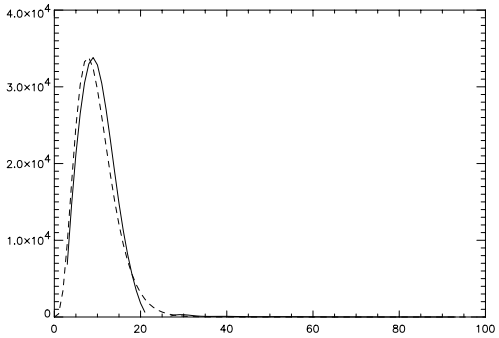

Mar

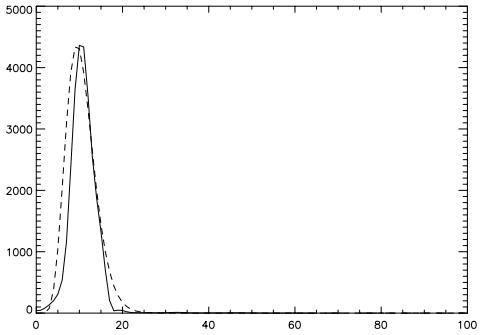

Apr

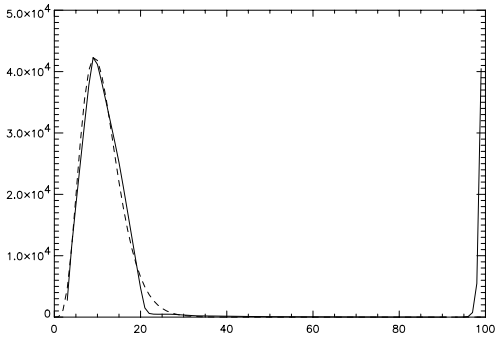

May

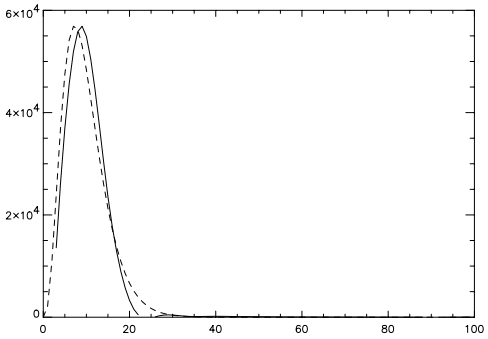

Jun

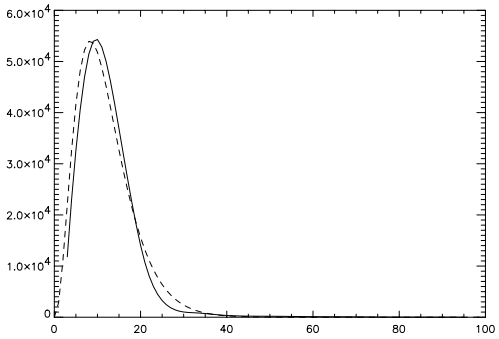

Jul

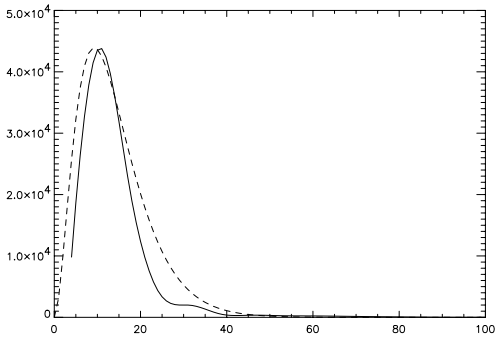

Aug

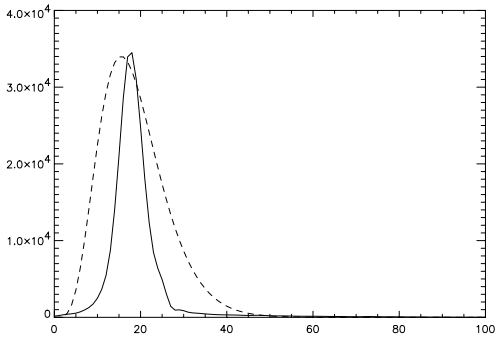

Sep

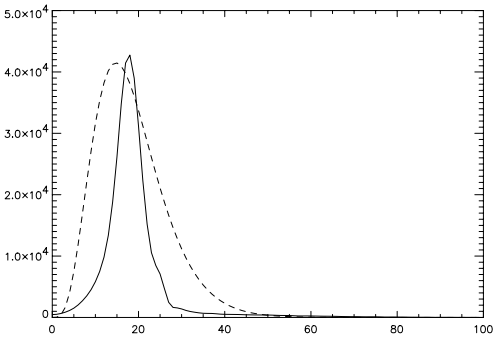

Oct

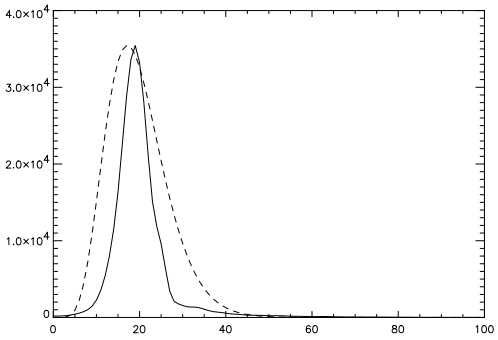

Nov

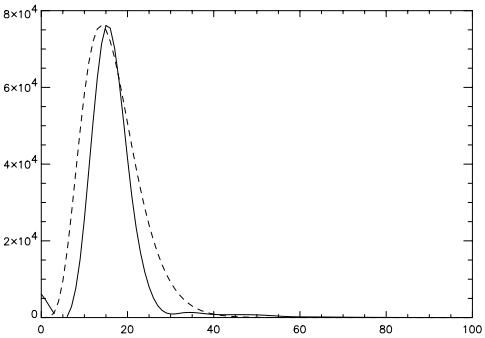

Dec

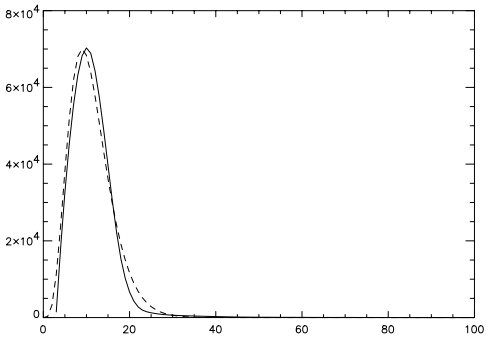

Appendix C: AVHRR imagery

In this appendix, AVHRR channel 1 and 4 images from April 2 are shown. The images have been rectified to a polar stereographic grid as shown below:

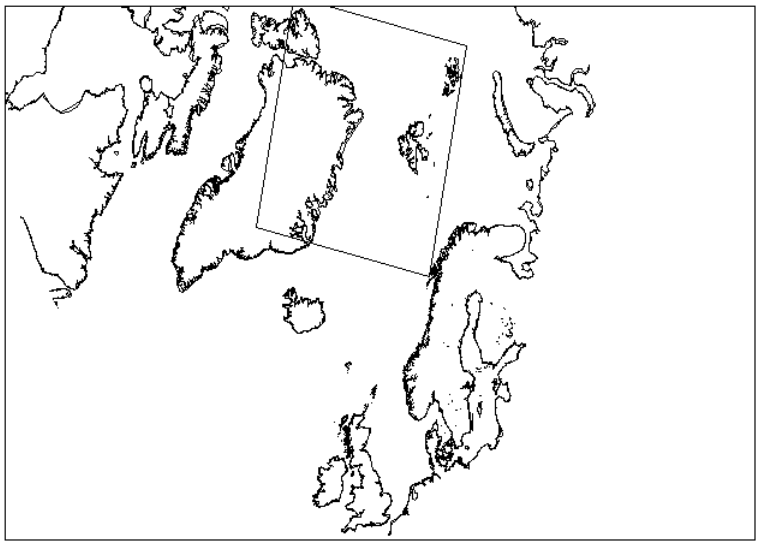

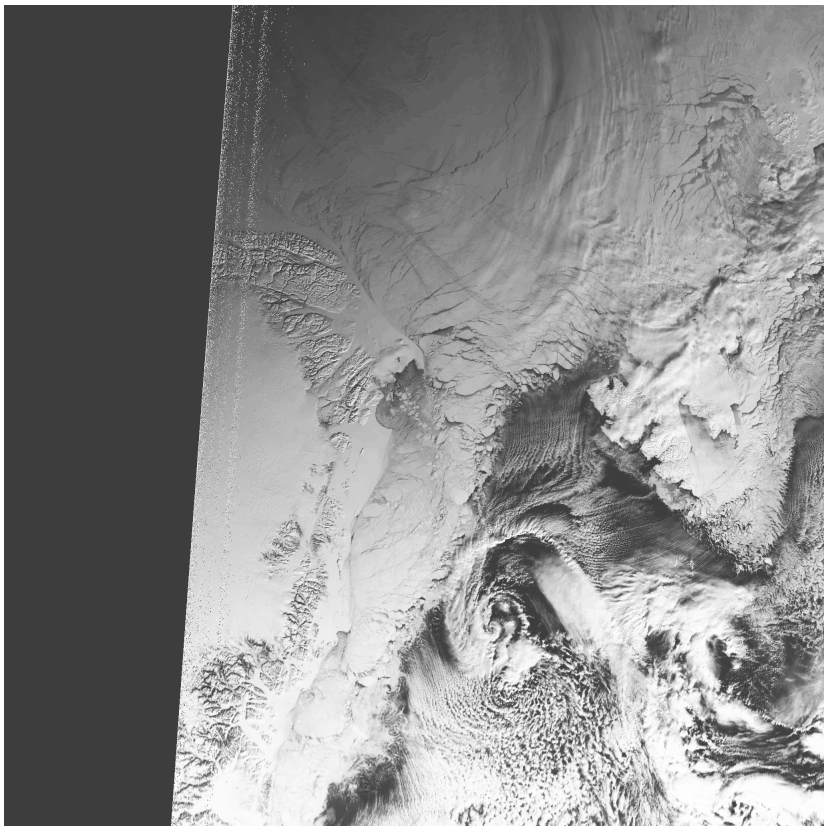

AVHRR channel 1, April 2 1999, 1050 UTC.

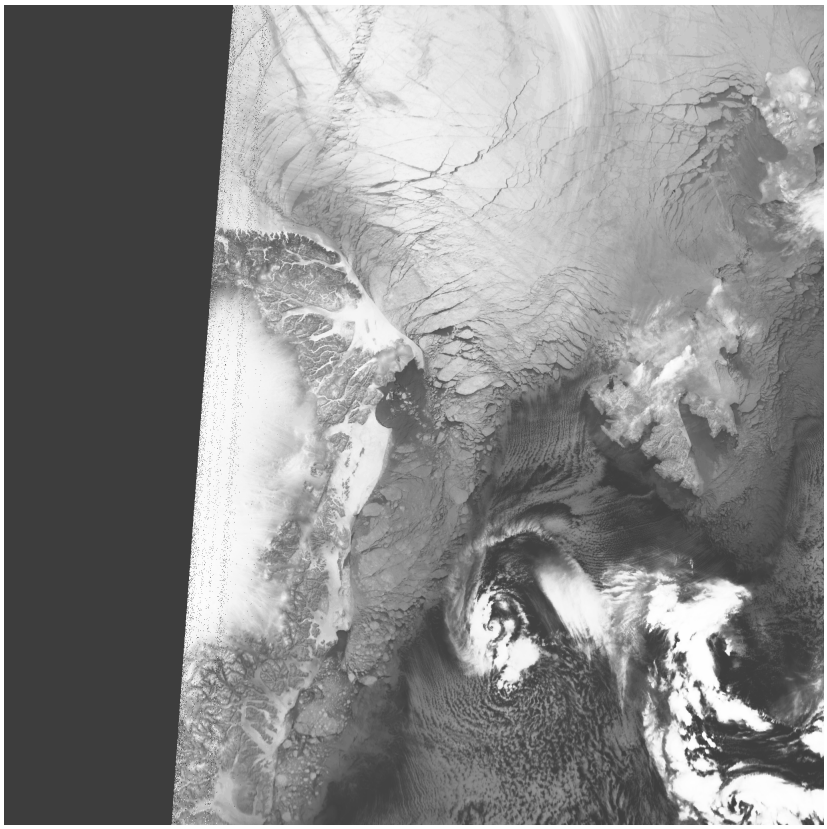

AVHRR channel 1, April 2 1999, 1050 UTC.

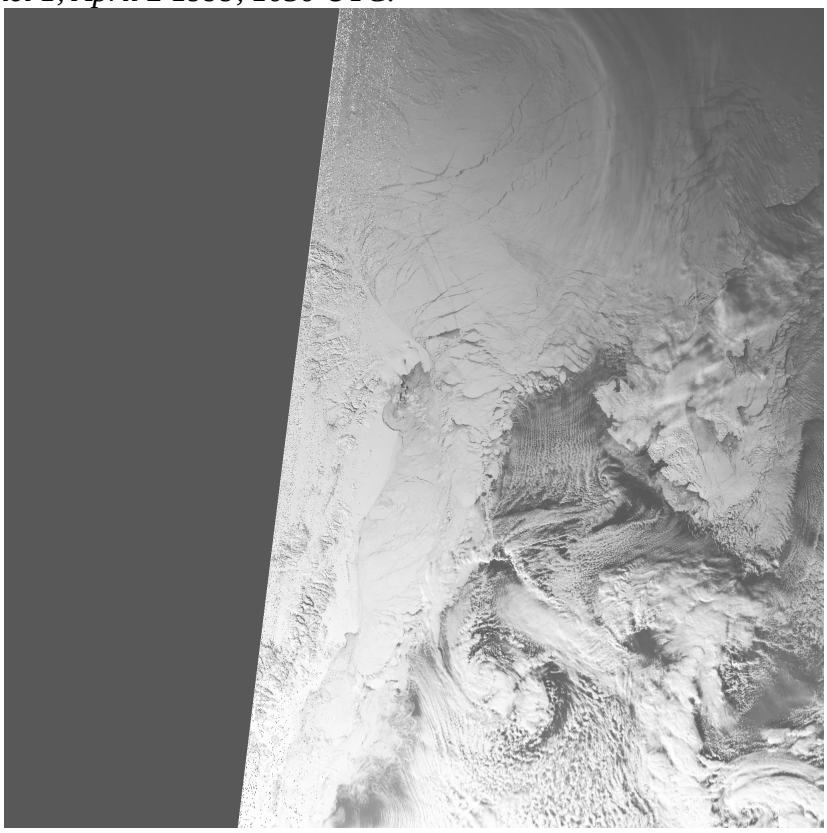

AVHRR channel 1, April 2 1999, 1435 UTC.

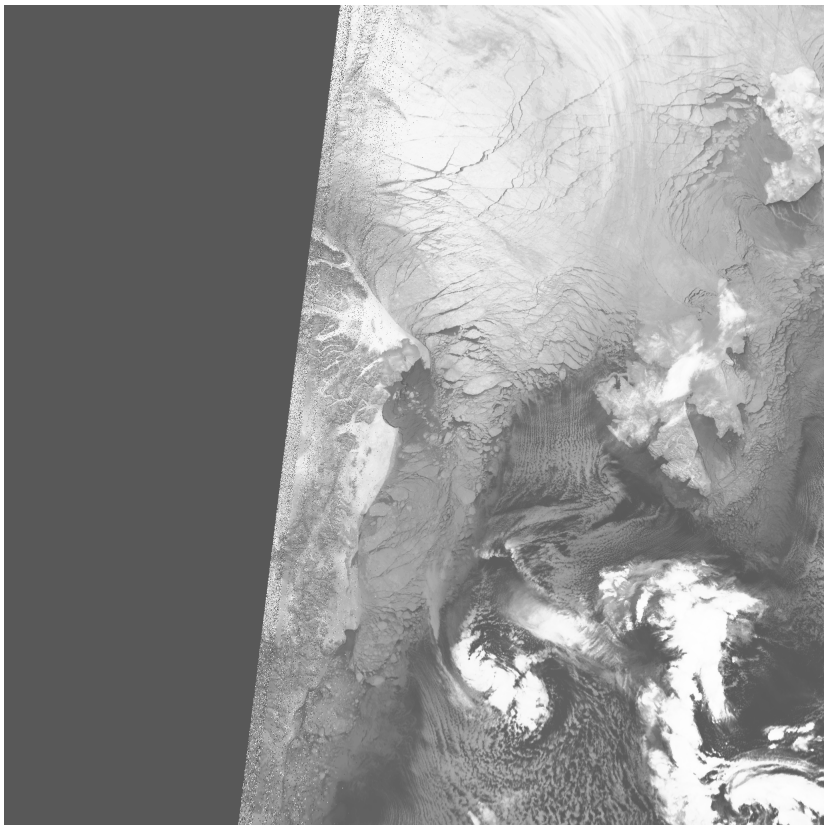

AVHRR channel 4, April 2 1999, 1435 UTC.

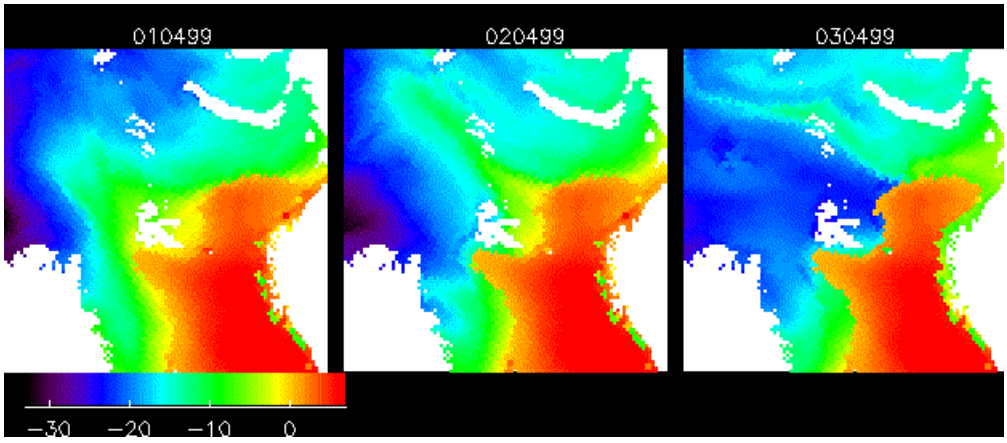

Near surface temperatures extracted from the HIRLAM NWP model running at DMI. Notice the intrusion of relatively mild air on April 1, that extends to the North Pole. On April 2 this air mass has moved East and is coincident with the yellow hues in Figure 6 stretching from the ice edge East of Svalbard across the Frans Josef Land archipelago to Severnaja Semlja.

DANISH METEOROLOGICAL INSTITUTE

Scientific Reports

Scientific reports from the Danish Meteorological Institute cover a variety of geophysical fields, i.e. meteorology (including climatology), oceanography, subjects on air and sea pollution, geomagnetism, solar-terrestrial physics, and physics of the middle and upper atmosphere.

Reports in the series within the last five years:

No. 95-1
Peter Stauning and T.J. Rosenberg:
High-Latitude, day-time absorption spike events
1. morphology and occurrence statistics
Not published

No. 95-2
Niels Larsen: Modelling of changes in stratospheric ozone and other trace gases due to the emission changes : CEC Environment Program Contract No. EV5V-CT92-0079. Contribution to the final report

No. 95-3
Niels Larsen, Bjørn Knudsen, Paul Eriksen, Ib Steen Mikkelsen, Signe Bech Andersen and Torben Stockflet Jørgensen: Investigations of ozone, aerosols, and clouds in the arctic stratosphere : CEC Environment Program Contract No. EV5V-CT92-0074. Contribution to the final report

No. 95-4
Per Høeg and Stig Syndergaard: Study of the derivation of atmospheric properties using radio-occultation technique

No. 95-5
Xiao-Ding Yu, **Xiang-Yu Huang** and **Leif Laursen** and Erik Rasmussen: Application of the HIRLAM system in China: heavy rain forecast experiments in Yangtze River Region

No. 95-6
Bent Hansen Sass: A numerical forecasting system for the prediction of slippery roads

No. 95-7
Per Høeg: Proceeding of URSI International Conference, Working Group AFG1 Copenhagen, June 1995. Atmospheric research and applications using observations based on the GPS/GLONASS System
Not published

No. 95-8
Julie D. Pietrzak: A comparison of advection schemes for ocean modelling

No. 96-1
Poul Frich (co-ordinator), H. Alexandersson, J. Ashcroft, B. Dahlström, G.R. Demarée, A. Drebs, A.F.V. van Engelen, E.J. Førland, I. Hanssen-Bauer, R. Heino, T. Jónsson, K. Jonasson, L. Keegan, P.Ø. Nordli, **T. Schmith**, **P. Steffensen**, H. Tuomenvirta, O.E. Tveito: North Atlantic Climatological Dataset (NACD Version 1) - Final report

No. 96-2
Georg Kjærgaard Andreasen: Daily response of high-latitude current systems to solar wind variations: application of robust multiple regression. Methods on Godhavn magnetometer data

No. 96-3
Jacob Woge Nielsen, Karsten Bolding Kristensen, Lonny Hansen: Extreme sea level highs: a statistical tide gauge data study

No. 96-4
Jens Hesselbjerg Christensen, Ole Bøssing Christensen, Philippe Lopez, Erik van Meijgaard, Michael Botzet: The HIRLAM4 Regional Atmospheric Climate Model

No. 96-5
Xiang-Yu Huang: Horizontal diffusion and filtering in a mesoscale numerical weather prediction model

No. 96-6
Henrik Svensmark and Eigil Friis-Christensen:
Variation of cosmic ray flux and global cloud coverage - a missing link in solar-climate relationships

No. 96-7
Jens Havskov Sørensen and Christian Ødum Jensen: A computer system for the management of epidemiological data and prediction of risk and economic consequences during outbreaks of foot-and-

mouth disease. CEC AIR Programme. Contract No. AIR3 - CT92-0652

No. 96-8
Jens Havskov Sørensen: Quasi-automatic of input for LINCOM and RIMPUFF, and output conversion. CEC AIR Programme. Contract No. AIR3 - CT92-0652

No. 96-9
Rashpal S. Gill and Hans H. Valeur:
Evaluation of the radarsat imagery for the operational mapping of sea ice around Greenland

No. 96-10
Jens Hesselbjerg Christensen, Bennert Machenhauer, Richard G. Jones, Christoph Schär, Paolo Michele Ruti, Manuel Castro and Guido Visconti:
Validation of present-day regional climate simulations over Europe: LAM simulations with observed boundary conditions

No. 96-11
Niels Larsen, Bjørn Knudsen, Paul Eriksen, Ib Steen Mikkelsen, Signe Bech Andersen and Torben Stockflet Jørgensen: European Stratospheric Monitoring Stations in the Artic: An European contribution to the Network for Detection of Stratospheric Change (NDSC): CEC Environment Programme Contract EV5V-CT93-0333: DMI contribution to the final report

No. 96-12
Niels Larsen: Effects of heterogeneous chemistry on the composition of the stratosphere: CEC Environment Programme Contract EV5V-CT93-0349: DMI contribution to the final report

No. 97-1
E. Friis Christensen og C. Skøtt: Contributions from the International Science Team. The Ørsted Mission - a pre-launch compendium

No. 97-2
Alix Rasmussen, Sissi Kiilsholm, Jens Havskov Sørensen, Ib Steen Mikkelsen: Analysis of tropospheric ozone measurements in Greenland: Contract No. EV5V-CT93-0318 (DG 12 DTEE): DMI's contribution to CEC Final Report Arctic Trophospheric Ozone Chemistry ARCTOC

No. 97-3
Peter Thejll: A search for effects of external events on terrestrial atmospheric pressure: cosmic rays

No. 97-4
Peter Thejll: A search for effects of external events on terrestrial atmospheric pressure: sector boundary crossings

No. 97-5
Knud Lassen: Twentieth century retreat of sea-ice in the Greenland Sea

No. 98-1
Niels Woetman Nielsen, Bjarne Amstrup, Jess U. Jørgensen:
HIRLAM 2.5 parallel tests at DMI: sensitivity to type of schemes for turbulence, moist processes and advection

No. 98-2
Per Høeg, Georg Bergeton Larsen, Hans-Henrik Benzon, Stig Syndergaard, Mette Dahl Mortensen: The GPSOS project
Algorithm functional design and analysis of ionosphere, stratosphere and troposphere observations

No. 98-3
Mette Dahl Mortensen, Per Høeg:
Satellite atmosphere profiling retrieval in a nonlinear troposphere
Previously entitled: Limitations induced by Multipath

No. 98-4
Mette Dahl Mortensen, Per Høeg:
Resolution properties in atmospheric profiling with GPS

No. 98-5
R.S. Gill and M. K. Rosengren
Evaluation of the Radarsat imagery for the operational mapping of sea ice around Greenland in 1997

No. 98-6
R.S. Gill, H.H. Valeur, P. Nielsen and K.Q. Hansen: Using ERS SAR images in the operational mapping of sea ice in the Greenland waters: final report for ESA-ESRIN's: pilot projekt no. PP2.PP2.DK2 and 2nd announcement of opportunity for the exploitation of ERS data projekt No. AO2..DK 102

No. 98-7
Per Høeg et al.: GPS Atmosphere profiling methods and error assessments

No. 98-8
H. Svensmark, N. Woetmann Nielsen and A.M. Sempreviva: Large scale soft and hard turbulent states of the atmosphere

No. 98-9
Philippe Lopez, Eigil Kaas and Annette Guldberg: The full particle-in-cell advection scheme in spherical geometry

No. 98-10
H. Svensmark: Influence of cosmic rays on earth's climate

No. 98-11
Peter Thejll and Henrik Svensmark: Notes on the method of normalized multivariate regression

No. 98-12
K. Lassen: Extent of sea ice in the Greenland Sea 1877-1997: an extension of DMI Scientific Report 97-5

No. 98-13
Niels Larsen, Alberto Adriani and Guido DiDonfrancesco: Microphysical analysis of polar stratospheric clouds observed by lidar at McMurdo, Antarctica

No.98-14
Mette Dahl Mortensen: The back-propagation method for inversion of radio occultation data

No. 98-15
Xiang-Yu Huang: Variational analysis using spatial filters

No. 99-1
Henrik Feddersen: Project on prediction of climate variations on seasonel to interannual timescales (PROVOST) EU contract ENVA4-CT95-0109: DMI contribution to the final report:Statistical analysis and post-processing of uncoupled PROVOST simulations

No. 99-2
Wilhelm May: A time-slice experiment with the ECHAM4 A-GCM at high resolution: the experimental design and the assessment of climate change as compared to a greenhouse gas experiment with ECHAM4/OPYC at low resolution

No. 99-3
Niels Larsen et al.: European stratospheric monitoring stations in the Artic II: CEC Environment and Climate Programme Contract ENV4-CT95-0136. DMI Contributions to the project

No. 99-4
Alexander Baklanov: Parameterisation of the deposition processes and radioactive decay: a review and some preliminary results with the DERMA model

No. 99-5
Mette Dahl Mortensen: Non-linear high resolution inversion of radio occultation data

No. 99-6
Stig Syndergaard: Retrieval analysis and methodologies in atmospheric limb sounding using the GNSS radio occultation technique

No. 99-7
Jun She, Jacob Woge Nielsen: Operational wave forecasts over the Baltic and North Sea

No. 99-8
Henrik Feddersen: Monthly temperature forecasts for Denmark - statistical or dynamical?

No. 99-9
P. Thejll, K. Lassen: Solar forcing of the Northern hemisphere air temperature: new data

No. 99-10
Torben Stockflet Jørgensen, Aksel Walløe Hansen: Comment on "Variation of cosmic ray flux and global coverage - a missing link in solar-climate relationships" by Henrik Svensmark and Eigil Friis-Christensen

No. 99-11
Mette Dahl Meincke: Inversion methods for atmospheric profiling with GPS occultations

No. 99-12
Benzon, Hans-Henrik; Olsen, Laust: Simulations of current density measurements with a Faraday Current Meter and a magnetometer

No. 00-01
Høeg, P.; Leppelmeier, G: ACE: Atmosphere Climate Experiment: proposers of the mission

No. 00-02
Høeg, P.: FACE-IT: Field-Aligned Current Experiment in the Ionosphere and Thermosphere

No. 00-03
Allan Gross: Surface ozone and tropospheric chemistry with applications to regional air quality modeling. PhD thesis

No. 00-04

Henrik Vedel: Conversion of WGS84 geometric heights to NWP model HIRLAM geopotential heights

No. 00-05
Jérôme Chenevez: Advection experiments with DMI-Hirlam-Tracer
(In Press)

No. 00-06
Niels Larsen: Polar stratospheric clouds micro-physical and optical models

No. 00-07
Alix Rasmussen: "Uncertainty of meteorological parameters from DMI-HIRLAM"
(In Press)

No. 00-08
A.L. Morozova: Solar activity and Earth's weather. Effect of the forced atmospheric trans-parency changes on the troposphere temperature profile studied with atmospheric models
(In Press)

No. 00-09
Niels Larsen, Bjørn M. Knudsen, Michael Gauss, Giovanni Pitari: Effects from high-speed civil traffic aircraft emissions on polar strato-spheric clouds
(In Press)